A SURVEY FOR CIRCUMSTELLAR DISKS AROUND YOUNG STELLAR OBJECTS

STEVEN V. W. BECKWITH
Department of Astronomy, Space Science Building, Cornell University, Ithaca, New York 14853

ANNEILA I. SARGENT
Department of Physics, Mathematics and Astronomy, California Institute of Technology, Pasadena, California 91125

ROLF. S. CHINI AND ROLF GÜSTEN
Max-Planck-Institute für Radioastronomie, Auf dem Hugel 69, D-5300 Bonn 1, Federal Republic of Germany
Received 6 July 1989; revised 3 November 1989

ABSTRACT

Continuum observations at 1.3 mm of 86 pre-main-sequence stars in the Taurus–Auriga dark clouds show that 42% have detectable emission from small particles. The detected fraction is only slightly smaller for the weak-line and "naked" T Tauri stars than for classical T Tauris, indicating that the former stars often have circumstellar material. In both categories, the column densities of particles are too large to be compatible with spherical distributions of circumstellar matter—the optical extinctions would be too large; the particles are almost certainly in spatially thin, circumstellar disks. Models of the spectral energy distributions from 10 to 1300 μm indicate that for the most part the disks are transparent at 1.3 mm, although the innermost ($\leqslant$1 AU) regions are opaque even at millimeter wavelengths. The aggregate particle masses are between 10^{-5} and 10^{-2} $\mathcal{M}_\odot$, implying total disk masses between 0.001 and 1 $\mathcal{M}_\odot$. The disk mass does not decrease with increasing stellar age up to at least 10^7 years among the stars detected at 1.3 mm. There is some evidence for temperature evolution, in the sense that older disks are colder and less luminous. There is little correlation between disk mass and Hα equivalent width among the detected stars, suggesting that the Hα line is not by itself indicative of disk mass. Spectral indices for several sources between 1.3 and 2.7 mm suggest that the particle emissivities ϵ are weaker functions of frequency ν than is the usual case of interstellar grains. Particle growth via adhesion in the dense disks might explain this result. The typical disk has an angular momentum comparable to that generally accepted for the early solar nebula, but very little stored energy, almost five orders of magnitude smaller than that of the central star. Our results demonstrate that disks more massive than the minimum mass of the proto-solar system commonly accompany the birth of solar-mass stars and suggest that planetary systems are common in the Galaxy.

I. INTRODUCTION

There is little doubt that the solar system was born from a disk of gas and dust encircling the Sun five billion years ago. The evidence that similar disks surround many young, solar-mass stars in the Galaxy today is compelling, although it is usually circumstantial. Basic quantities such as the disk mass are poorly constrained by available observations, however, making it impossible to ascertain the number of stars that will eventually have planetary systems like our own. If the distribution of mass and energy, the characteristics principally responsible for disk evolution, were known, we could begin to assess whether planetary systems are common or rare and, by comparing planetary evolution around neighboring stars, gain insight into our origins.

Most estimates suggest that approximately half of all young stars have disks. Strom *et al.* (1989; hereafter referred to as SSECS) use the presence of infrared emission in excess of that expected from a stellar photosphere to infer the presence of disks around 60% of the youngest pre-main-sequence stars in their sample. In a similar study, Cohen, Emerson, and Beichman (1989) examined 72 stars in Taurus–Auriga and concluded that about one-third of the stars have appreciable disks. Calculations of emission from circumstellar disks [Lynden-Bell and Pringle 1974; Adams, Lada, and Shu 1987 (hereafter referred to as ALS), 1988; Kenyon and Hartmann 1987; Bertout, Basri, and Bouvier 1988] demonstrate clear infrared signatures accompanying disks similar to the proto-solar nebula; these calculations provide the underpinnings for the observations cited above, but are not the only indicators of disk matter. The disks indirectly affect other radiation, for example, by shadowing the receding portions of stellar mass loss and creating preferentially blueshifted spectral lines (Edwards *et al.* 1987), asymmetric scattering of visual and near-infrared light from the stars (Beckwith *et al.* 1989), anomalously large extinction (Cohen 1983), and large degrees of polarization of the starlight (Bastien 1982; Hodapp 1984; Sato *et al.* 1985). But these effects are less useful for understanding the frequency with which disks occur.

At wavelengths shortward of 100 μm, these disks are usually opaque, making infrared and visual observations insensitive to the mass of the disks. The strengths of the far-infrared emission depends on the disks luminosity and temperature distribution, both strong functions of the energy balance in the disk (cf. Sec. IV*c*). To discuss the likelihood of planet formation, it is desirable to measure the total mass in a disk and its spatial distribution.

Thermal emission from small particles entrained in these disks is optically thin at wavelengths of order 1 mm and is proportional to the total particle mass (Beckwith *et al.* 1986; Sargent and Beckwith 1987). Observations of millimeter-wave emission from young stars provide an excellent way to measure disk masses directly, minimizing the uncertainties introduced by energetic activity near the star. With the unprecedented sensitivity and spatial resolution of the new

 0004-6256/90/030924-22$00.90

class of large, millimeter-wave telescopes and sensitive bolometer detectors, it is now possible to detect thermal emission from circumstellar disks with total masses only a few times that of Jupiter.

We present here the results of a survey for 1.3 mm radiation toward 86 stars in the Taurus–Auriga dark clouds. The sample contains classical T Tauri stars, stars in T associations identified from proper-motion surveys, and a few weak emission-line stars or naked T Tauri stars from x-ray selected samples. These stars are predominantly solar mass, well above the main sequence, with ages ranging from 10^5 to 10^7 yr. Our sensitivity was sufficient to detect particle masses of $\sim 10^{-4}\,\mathcal{M}_\odot$, corresponding to total masses of $0.01\,\mathcal{M}_\odot$, the minimum mass of the solar nebula at its birth.

II. SAMPLE

The sample is drawn from the works of Cohen and Kuhi (1979, hereafter referred to as CK79), Jones and Herbig (1979, hereafter referred to as JH79), Rydgren *et al.* (1984, hereafter referred to as RSZV), and Strom *et al.* (1986). These authors were primarily interested in classical T Tauri stars (TT) detected in Hα surveys, although RSZV include five x-ray selected stars from Walter and Kuhi (1981) and Feigelson and Kriss (1981). There is considerable overlap among the various compilations. Of the present sample, 35 are from CK79, 30 are from RSZV, and 22 are from JH79 only.

Because all these stars are in Taurus–Auriga, they are essentially at the same distance, which is assumed to be 140 pc (Elias 1978). There are probably 20% variations in distance within the sample owing to the finite size of the clouds; no attempt is made to place stars any more precisely.

Of the 86 sample stars, 20 are weak-line T Tauri stars (wTT). We adopt the definition of SSECS that stars with Hα equivalent widths less than 10 Å are classified as wTT. The Hα measurements are from Herbig and Robbin-Bell (1988), SSECS, and Jones (1988, personal communication). Taken as a subsample, the wTTs are useful to test the assertion that weak-line and naked T Tauri stars as a class have less circumstellar matter than their classical T Tauri counterparts (cf. Walter 1987; Walter, Brown, and Vrba 1989). A more general discussion of this problem is given by SSECS.

Table I lists the stars observed, the appropriate reference

TABLE I. Sample stars.

HBC	Name	Alt. Name	RA (1950)	Dec (1950)	Ref	Class	F_ν(mJy)	σ
23	FM Tau	Haro 6-1	04:11:07.9	+28 05 19	RSZV	TT	31	12
24	FN Tau	Haro 6-2	04:11:08.61	+28 20 26.9	JH79	TT	**31**	**9**
25	CW Tau	MHa 259-3	04:11:11.39	+28 03 26.8	JH79	TT	**96**	**8**
26	FP Tau	MHa 259-23	04:11:43.50	+26 38 57.5	JH79	TT	< 50	–
27	CX Tau	MHa 259-22	04:11:44.02	+26 40 42.2	JH79	TT	< 40	–
28	CY Tau	MHa 259-5	04:14:27.67	+28 13 28.6	JH79	TT	**133**	**11**
29	V410 Tau	BD+28 637	04:15:24.83	+28 20 01.7	JH79	wTT	< 30	–
30	DD Tau	MHa 259-6s	04:15:25.10	+28 09 14.6	JH79	TT	< 50	–
31	CZ Tau	MHa 259-6n	04:15:25.55	+28 09 44.0	JH79	wTT	< 30	–
32	BP Tau		04:16:08.61	+28 59 15.3	JH79	TT	37	15
33	DE Tau	MHa 259-8	04:18:49.84	+27 48 05.2	JH79	TT	**36**	**7**
34	RY Tau		04:18:50.8	+28 19 35.0	RSZV	TT	**229**	**17**
35	T Tau		04:19:04.21	+19 25 05.4	JH79	TT	**280**	**9**
36	DF Tau	MHa 259-11	04:23:59.63	+25 35 41.7	JH79	TT	< 25	–
37	DG Tau	MHa 259-10	04:24:01.01	+25 59 35.5	JH79	TT	**443**	**20**
38	DH Tau	MHa 259-9n	04:26:37.1	+26 26 29	RSZV	TT	53	19
39	DI Tau	MHa 259-9s	04:26:38.0	+26 26 21	RSZV	wTT	< 35	–
41	IQ Tau	LkHa 265	04:26:47.7	+26 00 17	RSZV	wTT	**87**	**11**
43	UX Tau A		04:27:09.96	+18 07 21.0	JH79	wTT	**73**	**14**
44	FX Tau	Haro 6-11	04:27:27.91	+24 20 18.2	JH79	wTT	20	10
45	DK Tau	MHa 259-12	04:27:40.48	+25 54 59.0	JH79	TT	**35**	**7**
46	ZZ Tau		04:27:49.32	+24 35 56.9	JH79	TT	< 15	–
47	V927 Tau	Lk Hα 331	04:28:22.39	+24 04 29.7	JH79	wTT	< 20	–
49	HL Tau	Haro 6-14	04:28:44.42	+18 07 36.2	JH79	TT	**879**	**19**
50	XZ Tau		04:28:46.00	+18 07 35.2	JH79	TT	17	6
48	HK Tau	Haro 6-12	04:28:48.85	+24 17 56.2	JH79	TT	**41**	**5**
51	V710 Tau	Lk Hα 266	04:29:03.57	+18 15 15.5	JH79	TT	**71**	**4**
54	GG Tau	MHa 257-2	04:29:37.2	+17 25 22	RSZV	TT	**593**	**53**
52	UZ Tau	UZ Tau f/p	04:29:39.26	+25 46 13.4	JH79	TT	**172**	**15**
55	GH Tau	Haro 6-20	04:30:04.8	+24 03 19	RSZV	TT	< 30	–
56	GI Tau	Haro 6-21	04:30:32.4	+24 15 04	RSZV	TT	< 20	–
59	IS Tau	Haro 6-23	04:30:32.66	+26 03 34.5	JH79	TT	< 20	–
57	GK Tau	Haro 6-22	04:30:32.8	+24 14 53	RSZV	TT	17	7
58	DL Tau	MHa 259-13	04:30:36.02	+25 14 24.0	JH79	TT	**230**	**14**
60	HN Tau	Haro 6-24	04:30:45.67	+17 45 38.2	JH79	TT	31	15
61	CI Tau	MHa 259-20	04:30:52.20	+22 44 16.7	JH79	TT	**190**	**17**
62	DM Tau	MHa 257-6	04:30:54.68	+18 03 56.7	JH79	TT	**109**	**13**
63	AA Tau	MHa 259-17	04:31:53.45	+24 22 44.1	JH79	TT	**88**	**9**
64	HO Tau	Haro 6-27	04:32:20.9	+22 26 06	RSZV	TT	< 30	–
65	DN Tau	MHa 259-18	04:32:25.68	+24 08 52.3	JH79	TT	**84**	**13**

TABLE I. (continued)

HBC	Name	Alt. Name	RA (1950)	Dec (1950)	Ref	Class	F_ν(mJy)	σ
66	HP Tau	Lk Hα 258	04:32:53.0	+22 48 18	CK79	TT	**62**	**6**
67	DO Tau	MHa 259-15	04:35:24.18	+26 04 55.2	JH79	TT	**136**	**11**
68	VY Tau		04:36:17.41	+22 42 02.3	JH79	wTT	< 50	-
69	V995 Tau	Lk Hα 332	04:39:04.4	+25 17 33	RSZV	TT	< 50	-
70	DP Tau	MHa 259-19	04:39:34.31	+25 09 59.9	JH79	TT	18	9
71	GO Tau	MHa 259-24	04:39:59.57	+25 14 43.0	JH79	TT	**83**	**12**
72	DQ Tau	MHa 257-7	04:43:59.99	+16 54 40.1	JH79	TT	**91**	**9**
74	DR Tau	MHa 257-8	04:44:13.4	+16 53 24	RSZV	TT	**159**	**11**
75	DS Tau	MHa 259-2	04:44:39.1	+29 19 56	RSZV	TT	**23**	**4**
76	UY Aur		04:48:35.71	+30 42 13.6	JH79	TT	**48**	**9**
77	GM Aur	MHa 259-1	04:51:59.8	+30 17 15	RSZV	TT	**253**	**12**
79	SU Aur		04:52:47.84	+30 29 19.4	JH79	wTT	21	10
367	V773 Tau	HD 283447	04:11:07.29	+28 04 41.2	JH79	wTT	**42**	**6**
369	FO Tau		04:11:43.60	+28 05 01.6	JH79	TT	< 50	-
373	V892 Tau	Elias 1	04:15:34.51	+28 12 01.8	JH79	Ae	**289**	**13**
374	Hubble 4		04:15:40.89	+28 12 54.0	JH79	wTT	< 25	-
377	FQ Tau	Haro 6-3	04:16:06.42	+28 22 21.4	JH79	TT	< 40	-
378	V819 Tau	WK X-Ray 1	04:16:20.1	+28 19 02	RSZV	wTT	**34**	**7**
383	FS Tau	Haro 6-5	04:18:57.63	+26 50 30.5	JH79	TT	< 35	-
384	FT Tau	Haro 6-6	04:20:37.23	+24 49 20.1	JH79	TT	**130**	**14**
386	FV Tau	Haro 6-8	04:23:49.85	+26 00 13.0	JH79	TT	36	15
396	Haro 6-13		04:29:13.6	+24 22 41	SSMW	TT	**124**	**13**
399	V827 Tau	FK X-Ray 2	04:29:20.6	+18 13 53	RSZV	wTT	< 30	-
400	V826 Tau	FK X-Ray 1	04:29:22.2	+17 55 17	RSZV	wTT	27	10
401	FY Tau	Haro 6-17	04:29:28.92	+24 13 38.6	JH79	TT	**16**	**5**
402	FZ Tau	Haro 6-18	04:29:30.08	+24 13 44.4	JH79	TT	**23**	**7**
405	V830 Tau	WK X-Ray 2	04:30:08.2	+24 27 26	RSZV	wTT	< 40	-
409	FF Tau		04:32:20.92	+22 48 16.8	JH79	wTT	26	9
416	Haro 6-28		04:32:55.8	+22 48 40	SSMW	TT	< 40	-
418	HV Tau		04:35:30.90	+26 04 45.2	JH79	wTT	30	15
420	IW Tau	S9557	04:38:01.94	+24 45 21.8	JH79	wTT	< 50	-
429	V836 Tau	FK X-Ray 3	05:00:02.4	+25 19 07	RSZV	wTT	**22**	**6**
	FR Tau	Haro 6-4	04:16:29.11	+28 20 11.5	JH79		< 50	-
	FU Tau	Haro 6-7	04:20:33.29	+24 56 08.3	JH79		< 35	-
	GT Tau		04:20:34.20	+24 48 21.9	JH79		< 35	-
	FW Tau		04:26:25.64	+26 10 22.0	JH79		< 15	-
	ZZ Tau B		04:27:14.62	+24 33 01.5	JH79	wTT	< 20	-
	IT Tau		04:30:50.47	+26 07 14.1	JH79		20	11
	HQ Tau		04:32:47.42	+22 44 16.1	JH79		< 45	-
	FG Tau		04:33:08.60	+23 56 50.8	JH79		< 45	-
	HD 283759		04:33:47.29	+24 06 57.5	JH79		< 35	-
	FI Tau		04:34:11.32	+23 30 16.3	JH79		< 50	-
	HT Tau		04:34:46.75	+26 18 00.9	JH79		< 50	-
	GN Tau	Haro 6-31	04:36:17.04	+25 39 11.2	JH79		< 50	-
	Haro 6-32		04:38:00.00	+25 52 12.2	JH79		< 50	-
	Haro 6-39		04:48:58.24	+30 32 47.3	JH79		**24**	**6**

Boldface is used to indicate detections of three standard deviations or greater. These detections were used for the statistics quoted in the text.

number in the Herbig and Robbin-Bell catalog (1988, hereafter referred to as HBC), the positions used in the survey, references for the positions, and the classification as TT or wTT when available. The positions of 65 of these stars were of astrometric quality, known to 0.1″ from JH79. The remainder can be found in Strom *et al.* (1986) or HBC. All the positions should be accurate to at least 1″.

Stellar properties—effective temperatures, luminosities, and so forth—exist in the literature for many of the stars in this sample and are given in Table II. Columns 1 and 2 are identical to those in Table I. Columns 3 through 7 list the spectral type, effective temperature, equivalent width of the Hα line, visual extinction, and stellar luminosity, respectively. Whenever possible, we calculated the extinctions and stellar luminosities based on a method described below; otherwise, data are from Cohen and Kuhi (1979) or Rydgren *et al.* (1984), corrected for the different assumed distances to the Taurus complex. We calculated the ages and masses of the stars from their positions in the *HR* diagram using convective tracks and isochrones kindly supplied by D. Vandenberg (cf. Vandenberg 1983); these are in columns 8 and 9 of Table II.

There are potentially large uncertainties in the calculated extinction, stellar luminosity, and bolometric luminosity for each star. We determined extinction by dereddening each star until the *color* of the blackbody corresponding to the stellar effective temperature fitted the *V* through *J* magnitudes in the least-squares sense; all magnitudes were taken

TABLE II. Star properties.

HBC	Object	SpT	Log(T_{eff})	WH_α[a]	Av[b]	L_*[c]	Log(t)[d]	M_*[e]
23	FM Tau	M0	3.593	71	2.7	0.6	6.32	0.67
24	FN Tau	M5	3.494	25	2.8	1.0	4.86	0.27
25	CW Tau	K3	3.679	135	2.6	2.6	6.28	1.40
26	FP Tau	M5.5	3.483	39	0.52	0.39	5.53	0.26
27	CX Tau	M2	3.566	20	1.45	0.58	5.95	0.46
28	CY Tau	M1	3.566	70	1.39	0.66	5.87	0.48
29	V410 Tau	K7	3.602	2	0.66	2.19	5.43	0.63
30	DD Tau	M1	3.566	182	2.7	1.0	5.54	0.46
31	CZ Tau	M1.5	3.555	4	2.55	0.38	6.13	0.40
32	BP Tau	K7	3.602	40	1.37	1.21	5.85	0.67
33	DE Tau	M1	3.566	54	1.62	1.21	5.40	0.44
34	RY Tau	K1	3.708	21	2.7	7.5	5.33	1.69
35	T Tau	K1	3.708	38	2.1	14.	5.27	1.91
36	DF Tau	M0.5	3.587	54	1.96	2.97	5.00	0.53
37	DG Tau	Cont	3.590	113	1.6	1.7	5.47	0.56
38	DH Tau	M0	3.593	53	2.39	0.84	6.04	0.67
39	DI Tau	M0	3.593	2	1.43	0.93	5.97	0.60
41	IQ Tau	M0.5	3.580	8	2.01	0.92	5.79	0.54
43	UX Tau	K2	3.695	4	1.8	2.7	6.42	1.49
44	FX Tau	M1	3.566	10	2.25	0.96	5.57	0.44
45	DK Tau	K7	3.602	19	2.01	1.94	5.52	0.65
46	ZZ Tau	M4	3.509	16	1.81	0.73	5.18	0.28
47	V927 Tau	M5.5	3.483	5	1.5	0.4	5.42	0.26
49	HL Tau	Cont	3.590	65	3.2	0.9	5.98	0.55
50	XZ Tau	M3	3.526	274	3.54	1.55	4.74	0.29
48	HK Tau	M0.5	3.580	29	3.99	0.76	5.94	0.55
51	V710 Tau	M1	3.566	48	2.66	1.60	5.18	0.42
52	UZ Tau	M1	3.566	82	2.86	2.94	4.74	0.44
54	GG Tau	K7	3.602	55	1.94	2.03	5.49	0.65
55	GH Tau	M2	3.544	15	1.06	0.88	5.33	0.33
56	GI Tau	K7	3.602	19	2.52	1.66	5.64	0.70
57	GK Tau	K7	3.602	16	1.8	1.6	5.64	0.67
58	DL Tau	Cont	3.590	105	1.53	0.77	6.08	0.56
59	IS Tau	K2	3.695	12	4.5	3.1	6.29	1.58
60	HN Tau	Cont	3.590	139	2.0	0.3	6.74	0.59
61	CI Tau	K7	3.602	102	2.33	1.14	5.90	0.70
62	DM Tau	M0.5	3.580	140	1.48	0.36	6.51	0.62
63	AA Tau	K7	3.602	37	1.10	0.98	6.01	0.67
64	HO Tau	M0.5	3.580	115	2.0	0.2	6.85	0.64
65	DN Tau	M0	3.593	12	1.19	1.12	5.81	0.62
66	HP Tau	K3	3.679	35	3.01	2.00	6.44	1.43
67	DO Tau	K7	3.602	109	3.43	1.38	5.78	0.72
68	VY Tau	M0	3.593	5	2.11	0.73	6.15	0.70
69	V995 Tau	K7	3.602	13	4.2	2.0	5.49	0.72

TABLE II. (continued)

HBC	Object	SpT	Log(T_{eff})	WH_α[a]	A_V[b]	L_*[c]	Log(t)[d]	M_*[e]
70	DP Tau	M0.5	3.580	86	2.24	0.54	6.20	0.60
71	GO Tau	M0	3.593	81	2.23	0.35	6.73	0.67
72	DQ Tau	K7	3.602	113	2.35	1.07	5.96	0.67
74	DR Tau	Cont	3.590	87	1.6	2.5	5.16	0.55
75	DS Tau	K3	3.679	59	1.43	1.32	6.78	1.29
76	UY Aur	K7	3.602	73	1.88	1.88	5.55	0.65
77	GM Aur	K7	3.602	97	0.5	0.7	6.25	0.72
79	SU Aur	G2III	3.761	4	1.45	14.4	4.48	2.65
367	V773 Tau	K2	3.695	2	2.10	7.68	5.71	1.74
369	FO Tau	M2	3.544	117	1.94	–	–	–
373	Elias 1	A6	3.907	13	4.5	0.7	7.63	1.03
374	Hubble 4	K7	3.602	3	0.77	–	–	–
377	FQ Tau	M2	3.544	114	1.12	–	–	–
378	V819 Tau	K7	3.602	2	1.94	0.95	6.06	0.72
383	FS Tau	M1	3.566	57	2.9	1.0	5.57	0.44
384	FT Tau	Cont	3.590	-	–	–	–	–
386	FV Tau	K5	3.643	23	4.83	–	–	–
396	Haro 6-13	Cont	3.590	88	6.70	2.1	5.10	0.55
399	V827 Tau	K7	3.602	2	1.24	1.30	5.80	0.67
400	V826 Tau	K7	3.602	2	1.05	1.13	5.90	0.67
401	FY Tau	K7	3.602	59	3.56	–	–	–
402	FZ Tau	Cont	3.590	204	–	–	–	–
405	V830 Tau	K7	3.602	3	0.77	0.81	6.20	0.70
409	FF Tau	K7	3.602	1	–	–	–	–
416	Haro 6-28	M5	3.494	92	1.82	–	–	–
418	HV Tau	M2	3.544	4	1.95	–	–	–
420	IW Tau	K7	3.602	4	1.24	1.01	6.00	0.65
429	V836 Tau	K7	3.602	9	1.47	0.65	6.35	0.75
	FR Tau	–	–	-	–	–	–	–
	FU Tau	–	–	-	–	–	–	–
	GT Tau	–	–	-	–	–	–	–
	FW Tau	–	–	-	–	–	–	–
	ZZ Tau B	–	–	-	–	–	–	–
	IT Tau	–	–	-	–	–	–	–
	HQ Tau	–	–	-	–	–	–	–
	FG Tau	–	–	-	–	–	–	–
	HD 283759	–	–	-	–	–	–	–
	FI Tau	–	–	-	–	–	–	–
	HT Tau	–	–	-	–	–	–	–
	GN Tau	–	–	-	–	–	–	–
	Haro 6-32	–	–	-	–	–	–	–
	Haro 6-39	–	–	-	–	–	–	–

[a] Angstroms
[b] Magnitudes
[c] $L_\odot$
[d] t in years
[e] $M_\odot$

from SSECS. Then the stellar luminosity was varied to give the best overall fit. Most of these determinations are in accord with those of SSECS, who use only the $V - R$ color to determine A_V and subsequently fit to the R magnitude to determine stellar luminosity. For some stars, the extinction determined from fits to several wavelengths is larger than found by SSECS, indicating larger stellar luminosities. We believe the use of several wavelengths, rather than just two, provides a more satisfactory method for finding A_V and have used the more extensive fits whenever possible.

In general, stars with small visual extinctions should have well-determined luminosities. Stars that show continuum plus line emission (Cont in column 3) have the largest uncertainties and usually the largest extinctions. Cohen and Kuhi (1979) and Cohen, Emerson, and Beichman (1989) estimate stellar luminosities by correcting the flux densities for extinction (independently determined) and integrating the observed energy distribution. Usually the three methods give similar values, with the SSECS estimates being systematically smaller. The differences are not great and should not affect the conclusions in this paper.

The sample is almost certainly incomplete in the sense that there are young stars in the associations that do not appear in any of these lists. Herbig and Robbin-Bell (1988) show that Hα surveys miss stars in the post-T Tauri phase and do not provide adequately complete samples of pre-main-sequence stars in any dark cloud. The sample is probably representative of classical T Tauri variables, few of which should have been missed in the objective prism surveys, but does not necessarily represent all low-mass pre-main-sequence stars.

III. OBSERVATIONS

Observations of 1.3 mm continuum emission were made using the Max-Planck-Institute für Radioastronomie (MPIfR)[3] He-cooled bolometer (Kreysa 1984) at the IRAM 30 m telescope on Pico Veleta (Baars *et al.* 1987) during 29 and 30 April 1988. The instrument has a beam size of 11″ with a bandpass of 50 GHz (0.24 mm) centered at 1.3 mm. Chopping by 30″ at 8.5 Hz provided sky subtraction and effectively discriminated against emission more extended than the beam. Sky noise limited the system performance, owing to variations in the telluric opacity at the chopping frequency, but the weather was generally good throughout the observing sessions.

The survey was carried out in three separate passes, and each object was observed at least twice on separate days. A typical observation consisted of about ten measurements, each one a pair of differences between the two chopped beams on the sky. Statistical deviations of the measurements determined the system noise. The total integration time for each observation was 200 s.

Observations of the planets Mars and Uranus were used to calibrate the flux density scale. These observations were consistent to within 20%. Final flux densities of the objects were the calibrated averages of the separate observations, as described above.

A few of the strongest sources have been independently observed at wavelengths near 1.3 mm. Flux densities for HL Tau and DG Tau determined from observations with the Owens Valley Interferometer at 1.4 mm are in excellent agreement with those presented here, being within 5% in each case (Woody *et al.* 1989). In addition, V410 Tau, T Tau, DG Tau, HL Tau, HP Tau, DO Tau, GM Aur, and SU Aur have been observed at 1.1 mm in an 18″ beam at the JCMT (Weintraub, Sandell, and Duncan 1989; Adams, Emerson, and Fuller 1989). Within the uncertainties, their fluxes are in good agreement with those presented here.

We checked for extended emission near three of the brightest objects. Continuous cross scans of the stars HL Tau, GG Tau, and DG Tau showed no emission outside of the 11″ beam, giving confidence that the emission was unresolved in all cases. Indeed, interferometric observations of HL Tau, DG Tau, and GG Tau (Sargent and Beckwith 1987, 1990) at 2.7 mm demonstrate the continuum emission from these stars is smaller than the 5″ resolution of the interferometer beam. Weintraub, Sandell, and Duncan (1989) suggest the emission from DG Tau and HL Tau is more extended. Observations with higher spatial resolution and sensitivity, as well as more recent JCMT observations (Adams, Emerson, and Fuller 1989), do not support this contention.

IV. RESULTS

a) Statistics of Detections

The survey results appear in columns 8 and 9 of Table I which list the 1.3 mm flux density or an upper limit observed toward each star in the sample, and the statistical uncertainty. To qualify as a detection, the observed flux density must be at least three standard deviations (3σ) above zero. Each star was observed at least twice; it was found that every star whose flux density is approximately 3σ in the final average was at least 2σ in each of the two separate observations, giving confidence that the detection criteria discriminated against spurious results.

Thirty-seven stars in the sample, 42%, pass the formal detection criterion. Because the uncertainty σ was not constant throughout the sample, owing to time-variable telluric opacity, there is no uniform lower limit to the flux density. A few formal detections—FY Tau, FZ Tau, DS Tau, Haro 6-39, and V836 Tau—have very low flux densities, whereas DH Tau, with a relatively high flux density but also high uncertainty, is a nondetection. Even if these five stars are discounted, the detection rate is still fairly high, 36%.

Among the two subclasses, 28 of 53 (53%) T Tauris and six of 21 (29%) wTTs are detected. These percentages are very similar to those found by SSECS from their study of far-infrared properties. The T Tauris are by far the brightest stars at millimeter wavelengths, and most of the wTTs have relatively low flux densities. In fact at 1.3 mm, the brightest wTT, IQ Tau, is fully ten times less luminous than the brightest TT, HL Tau. We will show in Sec. IV*c* that the detectability of emission from the wTTs is related to the relatively cool temperatures of their circumstellar matter.

b) Nature of the Emission

It was assumed at the outset that the millimeter continuum flux is thermal emission from small particles and that these particles are embedded in disks of dust and gas surrounding the stars. For the bright sources HL Tau and DG Tau, these interpretations have been clearly established by Beckwith *et al.* (1986) and Sargent and Beckwith (1987, 1989). There are insufficient data to confirm these assumptions for every star, but we can show they are strongly supported for many in the sample and are quite likely to apply to all the members.

A likely alternative to thermal radiation is free–free emission from the ionized regions near the stars, since most of these stars do show Hα in emission. Figure 1 is a plot of F_ν at 1.3 mm vs Hα equivalent width, WHα, of the 1.3 mm detections. It can be seen that there is no correlation between F_ν and WHα. Since WHα should reflect the strength of free–free emission, it appears unlikely that this makes a significant contribution to the 1.3 mm flux.

Using the VLA, Bieging, Cohen, and Schwartz (1984) surveyed 44 stars in Taurus for 6 cm radio emission and followed up with 1.3–21 cm observations for some of the detected stars. Our sample includes 27 of these objects. V410 Tau, T Tau, and DG Tau showed 6 cm emission in excess of 500 μJy. The two brightest objects at 1.3 mm, HL Tau and GG Tau, were not detected.

V410 Tau is by far the strongest radio source with a 2.1 cm flux density of 64 mJy; it is reported to be variable by Bieging, Cohen, and Schwartz (1984). It was not detected in our 1.3 mm survey with an upper limit of 30 mJy. The spectrum turns over at 2.1 cm, as indicated by the VLA observations, and the 1.3 mm result is consistent with the centimeter-wave flux densities, assuming optically thin free–free emission. We emphasize that of the objects observed with the VLA, this star is the most likely to produce free–free emission at 1.3 mm, but it was not detected.

T Tau is the next strongest radio source with a 2.1 cm flux density of 7.5 mJy, which comes mainly from the infrared companion. Using the VLA data presented by Bieging, Cohen, and Schwartz (1984), making the most liberal assumptions about spectral index for T Tau itself, and extrapolating to 1.3 mm, we find the star can contribute at most 70 mJy, about 25% of the actual flux density. Weintraub, Masson, and Zuckerman (1989) argue that no more than 20% of the continuum emission at 2.7 mm can be free–free emission from the star. If all 280 mJy at 1.3 mm were free–free emission, the infrared hydrogen recombination lines Bα and Bγ would be 4.9×10^{-15} and 1.7×10^{-15} W m^{-2}, respectively. The actual lines fluxes are 1.6×10^{-15} and 7×10^{-16} W m^{-2} (e.g., Evans *et al.* 1987).

DG Tau has a total flux density of 1.2 mJy at 6 cm with a spectral index of 0.55 ± 0.32. In the extreme case of $\alpha = 0.87$, the 1.3 mm flux density would be 36 mJy, about 8% of the observed value. Radio free–free emission cannot contribute more than a small fraction of the millimeter-wave luminosity.

The other 24 sources that appear in both samples have 6 cm fluxes less than $\sim$ 500 μJy. Of the fifteen sources with 1.3 mm flux densities above 100 mJy, eight were observed at 6 cm. With the exception of T Tau and DG Tau, none were detected. If the 6 cm flux densities were 500 μJy for these stars, their spectral indices would have to be greater than one to produce the lowest 1.3 mm flux densities detected, 25 mJy. Even in an outflowing wind, free–free emission will not produce such steep spectra, and we conclude that for the stars in our sample there is no free–free contribution to the 1.3 mm emission.

Based on these considerations, we believe it unlikely that any of the 20 strongest sources [F_ν(1.3 mm) $\gtrsim$ 80 mJy] have substantial free–free emission. For a few of the weak sources, especially the wTTs, variable nonthermal radio emission could, in principle, provide the observed millimeter continuum. We assume this is not the case, however, and that the thermal emission from small particles produces the millimeter-wave continuum from all stars.

c) Particle Distribution

Most of the stars detected in the survey have 1.3 mm flux densities greater than 50 mJy, corresponding to a beam-averaged brightness temperature T_b of 0.014 K. The stellar luminosity is, in all cases, sufficient to make the particle temperatures much higher than this. Therefore, the emission is either very compact, the low brightness temperatures resulting from beam dilution, or optically thin.

Suppose the particles are distributed spherically around the star with some density distribution $\rho(r)$, which is a function only of distance r from the star, and the particles are optically thin at all wavelengths. We assume the particle

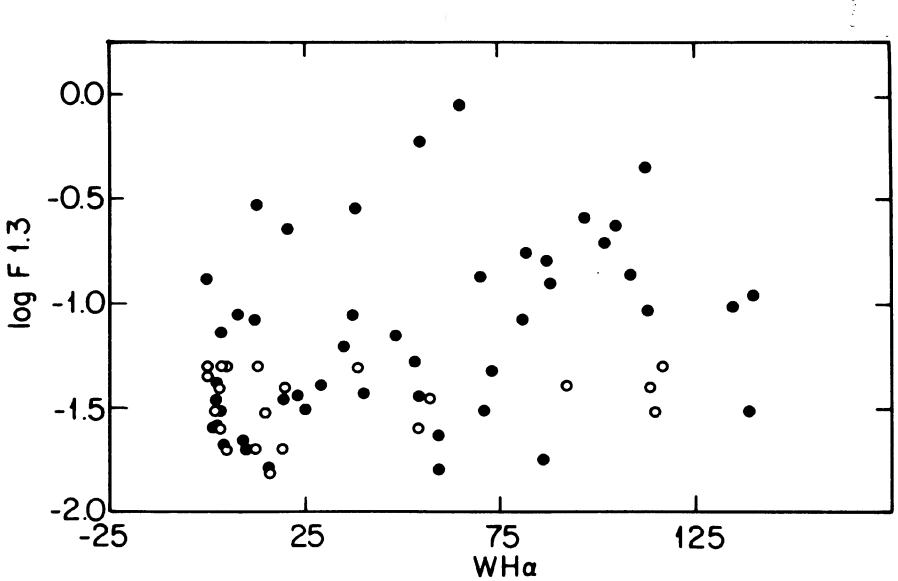

FIG. 1. 1.3 mm flux density F_ν is plotted against the equivalent width of the Hα line. The solid circles represent stars detected at 1.3 mm; the open circles with vertical lines are upper limits. The figure demonstrates no correlation between the 1.3 mm continuum emission and the emission-line strength, indicating that ionized gas is not responsible for the 1.3 mm flux density.

opacity κ_ν is a power law in frequency at low frequencies: $\kappa_\nu \propto \nu^\beta$. For small particles in radiative equilibrium with a star, the particle temperature will be (cf. Spitzer 1978)

$$T_p = \left(\frac{1}{2}\frac{R_*}{r}\right)^{2/(4+\beta)} T_*. \quad (1)$$

The stellar radius is R_*, and the stellar effective temperature is T_*. The flux density at 1.3 mm is

$$F_\nu = \frac{\Omega_B \kappa_\nu}{\pi R^2}\int_{r_0}^{R} B_\nu(T_p)\rho(r)4\pi r^2 dr, \quad (2)$$

where Ω_B is the solid angle of the beam, R is the beam radius (700 AU at the distance to Taurus), r_0 is the inner radius of the region, B_ν is the blackbody function, and κ_ν is the mass opacity at 1.3 mm. Writing $T_p(r) = T_0\ (r/r_0)^{-0.4}$ (i.e., $\beta = 1$), $\rho(r) = \rho_0(r/r_0)^{-s}$, assuming $s \neq 2.6$, and using the Rayleigh–Jeans approximation for B_ν, Eq. (2) becomes

$$F_\nu = \frac{1}{2.6-s}\frac{8\Omega_B\kappa_\nu\nu^2}{c^2}kT_0\rho_0 r_0^3\left[\left(\frac{R}{r_0}\right)^{2.6-s} - 1\right]. \quad (3)$$

The column density N toward the star is

$$N = \int_{r_0}^{R}\frac{\rho(r)}{\bar{m}}dr = \frac{\rho_0 r_0}{\bar{m}}\frac{1}{1-s}\left[\left(\frac{R}{r_0}\right)^{1-s} - 1\right], \quad (4)$$

where the average mass per particle is $\bar{m}$. Combining Eq. (2) and (3), the column density may be expressed in terms of the flux density as

$$N = \frac{2.6-s}{1-s}\frac{c^2 F_\nu}{8\Omega_B\kappa_\nu\nu^2\bar{m}kT_0}\frac{(R/r_0)^{1-s}-1}{r_0^2[(R/r_0)^{2.6-s}-1]}. \quad (5)$$

A typical star has a luminosity of about $1L_\odot$ (columns 7 and 4, Table II). If $r_0 = 0.1$ AU, then $T_0 \approx 1200$ K, close to the dust destruction temperature. We adopt $\kappa_\nu = 0.02$ cm^2 g^{-1} at 1.3 mm as an upper limit (discussed extensively in Sec. IV*e*), $\Omega_B = 1.8\times10^{-9}$ sr, and $\bar{m} = 4\times10^{-24}$ g, so the resulting column density will be mainly that of hydrogen. Using a typical flux density $F_\nu \sim 100$ mJy, the column density may be calculated for different density distributions specified through the exponent s. For $s = 0$ (uniform density, $N \sim 6\times10^{21}$ cm^{-2}, corresponding to a visual extinction A_V of 3 mag (Spitzer 1978). Freely falling accretion onto the star produces a density distribution with $s = \frac{3}{2}$, yielding A_V of 220 mag for the typical star. A uniform velocity stellar wind gives $s = 2$ and $N = 1\times10^{25}$ cm^{-2}, and a visual extinction of about 5100 mag.

Only a few of the objects in the sample have A_V as high as 3 mag, and none have A_V greater than 7 mag (column 6, Table II). Since the adopted value of κ_ν is higher by a factor of 5 than the usual value for interstellar particles, the large 1.3 mm flux densities clearly rule out spherical distributions of particles, unless the density *increases* with distance from the star ($s < 0$). But there is no correlation between visual extinction A_V and F_ν(1.3 mm) (e.g., Tables I and II), making it highly unlikely that the particles surround the stars completely. Because the most likely distribution would come about via infall ($s = \frac{3}{2}$) or outflow ($s = 2$), the predicted column densities are enormously higher than allowed by the observed small values of A_V.

The particles must be distributed very nonuniformly around each star to account for the simultaneously low visual extinctions and high flux densities at 1.3 mm. The most natural distribution is a highly flattened disk. In principle, the disks could even be optically thick at millimeter wavelengths and the stars would still be visible, except in the rare case where the disk was viewed edge on. Since such distributions are expected in realistic models of cloud collapse, in the rest of the paper we assume that the particles are in thin disks.

d) Analysis of Disk Structure

For the purposes of this study, the two most important global properties of a disk are its mass and temperature distribution. Both can be calculated from the far-infrared and millimeter-wave spectra. ALS have shown that infrared spectra of T Tauri stars may be fitted by assuming spatially thin disks and using numerical models of disk emission with several adjustable parameters. This section will demonstrate that only a few of the parameters significantly affect the emission spectra, and that it is possible to determine properties such as the temperature distribution and total mass of a disk from observations, with only minor uncertainties being introduced by unknown free parameters.

We assume the particles are in spatially thin, axisymmetric disks, with the temperature $T(r)$ and surface density $\Sigma(r)$ functions only of the radial distance from the star. Following ALS, we calculate the luminosity density $L_\nu = 4\pi D^2 \nu F_\nu$, where F_ν is flux density at distance D from the source. If the disk has inner and outer radii r_0 and R_d, respectively, and is inclined by angle θ to the line of sight ($\theta = 0$ is face on), then

$$L_\nu = 4\pi\cos\theta\int_{r_0}^{R_d}\nu B_\nu(T)(1-e^{-\tau_\nu})2\pi r dr. \quad (6)$$

B_ν is the usual Planck function, and the optical depth τ_ν is

$$\tau_\nu(r) = \kappa_\nu\Sigma(r)/\cos\theta. \quad (7)$$

Specification of r_0, R_d, κ_ν, θ, $T(r)$, and $\Sigma(r)$ completely characterizes the emission from the disk.

There are two wavelength regimes where L_ν is sensitive to only a few of the disk parameters, and it is possible to derive disk properties directly from the observations. At short wavelengths, the entire disk is optically thick, and the density distribution does not affect the emission. Similarly, at long wavelengths, the disk is optically thin, and the total emission is proportional to a product of the temperature and total mass, weighted appropriately by the distribution. To simplify the calculations, one can adopt power law radial dependencies for the temperature and density distributions and derive the essential parametric dependencies of the emission in the two regimes. In the remainder of the paper, we adopt power law forms for $T(r)$ and $\Sigma(r)$:

$$T(r) = T_0(r/r_0)^{-q}, \quad (8)$$

$$\Sigma(r) = \Sigma_0(r/r_0)^{-p}. \quad (9)$$

Because dust particle opacities increase with frequency, the disk will be optically thick at all radii for frequencies greater than some turnover frequency ν_d, and the factor $(1-e^{-\tau_\nu})$ is essentially unity. The turnover frequency ν_d corresponds to a wavelength of order 100 μm for the disks considered here. For a large range of frequencies greater than ν_d, the emission near the disk boundaries is negligible compared to the emission from intermediate radii ($r_0 \ll r \ll R_d$), and the limits of the integration may be safely

replaced with 0 and ∞, allowing the essential scaling relationships in Eq. (6) to be written explicitly:

$$L_\nu \approx A_0 \cos\theta\, Q(q)\,(T_0 r_0^q)^{2/q} \nu^{4-2/q}, \tag{10}$$

with the constant,

$$A_0 = 16\pi^2 h (k/hc^2)^{2/q}, \tag{11}$$

and the function,

$$Q(q) \equiv \int_0^\infty \frac{x}{e^{x^q}-1} dx. \tag{12}$$

The physical constants h, k, and c retain their usual values. In this region of the spectrum, L_ν is a *power law* with spectral index $4 - 2/q$. The index q is uniquely determined from the spectral index at wavelengths where the opacity is high ($\lambda \lesssim 100\,\mu$m), and the magnitude of L_ν accurately specifies $T_0 r_0^q$, and therefore $T(r)$; the dependence on θ is weak until $\theta \sim 90°$. The far-infrared spectral energy distribution thus provides a good measure of the disk temperature as a function of radius.

At very low frequencies, $\nu \ll \nu_d$, the disks are predominantly transparent, and the thermal emission is in the Rayleigh–Jeans limit. Equation (6) becomes

$$L_\nu \approx 16\pi^2 \cos\theta \left(\frac{k\nu^3}{c^2}\right) \int_{r_0}^{R_d} T(r)\,(1 - e^{-\tau_\nu}) r dr$$

$$\approx A_1 \cos\theta T_0 r_0^q \int_{r_0}^{R_d} r^{1-q} (1 - e^{-\tau_0 (r_0/r)^p}) dr, \tag{13}$$

with

$$A_1 = 16\pi^2 (k\nu^3/c^2). \tag{14}$$

We can approximate the integral in Eq. (13) by separating it into two parts, one for the portion of the disk where $\tau_\nu \geqslant 1$, and one for the portion where $\tau_\nu < 1$. Since the density decreases with radius for all realistic disks ($p > 0$), the inner part will be optically thick and the outer part optically thin with the boundary occurring at r_1, defined as

$$r_1 = \tau_0^{1/p} r_0 \tag{15a}$$

$$= (\kappa_\nu \Sigma_0 / \cos\theta)^{1/p} r_0 \tag{15b}$$

$$\approx [(2-p)/2]^{1/p} \bar{\tau}^{1/p} R_d. \tag{15c}$$

In deriving these results, we assume $R_d/r_0 \gg 1$. The disk mass M_d is related to Σ_0 by integrating Eq. (9). The average disk opacity $\bar{\tau}$ is defined as

$$\bar{\tau} \equiv \frac{\kappa_\nu M_d}{\cos\theta\, \pi R_d^2}. \tag{16}$$

Notice that r_1 depends only weakly on the choice of R_d for a given disk mass M_d; if $p \sim 1.5$, then $r_1 \sim R_d^{-1/3}$.

Equation (13) may now be approximated by letting $(1 - e^{-\tau_\nu}) = 1$ for $r \leqslant r_1$ and $(1 - e^{-\tau_\nu}) = \tau_\nu$ for $r \geqslant r_1$:

$$L_\nu \approx A_1 f_0 \cos\theta\, T_0 r_0^q \times \left(\int_{r_0}^{r_1} r^{1-q} dr + \tau_0 r_0^p \int_{r_1}^{R_d} r^{1-p-q} dr \right)$$

$$\approx A_1 f_0 \cos\theta\, T(r_1) r_1^2 \frac{(R_d/r_1)^{2-p-q} - 1}{2-p-q} (1 + \Delta). \tag{17}$$

The factor f_0 accounts for the extra luminosity that results from ignoring the curvature in the function $(1 - e^{\tau_\nu})$; for $f_0 \approx 0.8$, the results given by Eq. (17) and numerical integrations of Eq. (13) correspond very well. The factor Δ is the ratio of optically thick to optically thin emission and is discussed in detail below. For most of the stars in this paper, $\Delta < 1$. The exponent $2 - p - q$ is small for the temperature and density distributions most frequently assumed in the literature (e.g., ALS). For $q = 0.5$ (flat spectrum objects) and $p = 1.5$, the exponent is zero; in this limit, the luminosity depends only logarithmically on R_d/r_1:

$$L_\nu \approx A_1 f_0 \cos\theta\, T(r_1) r_1^2 \ln(R_d/r_1)(1 + \Delta). \tag{18}$$

The luminosity is dominated by the emission near the $\tau_\nu = 1$ radius, r_1. It is noteworthy that the choice of the inner boundary r_0 is irrelevant so long as $r_0 \ll r_1$. The dependence on disk mass and outer radius enters through $T(r_1)\, r_1^2$ which can be explicitly expanded as

$$T(r_1) r_1^2 \approx T_0 r_0^q r_1^{2-q}$$

$$\approx T_0 r_0^q \left(\frac{2-p}{2} \frac{\kappa_\nu}{\cos\theta} \frac{M_d}{\pi R_d^2} \right)^{(2-q)/p} R_d^{2-q}$$

$$\propto \frac{1}{\cos\theta} (\kappa_\nu M_d)^{(2-q)/p} R_d^{[(2-q)/p](p-2)}. \tag{19}$$

The luminosity dependence approaches $L_\nu \propto \kappa_\nu M_d \ln(M_d) R_d^{p-2}$ as $2 - p - q$ approaches 0. Furthermore, when the emission is optically thin, the $\cos\theta$ dependence vanishes in the relation between L_ν and M_d.

Formally, the calculations require specification of eight parameters (M_d, r_0, R_d, T_0, q, p, θ, and κ_ν). However, at long wavelengths where the average opacity is small, the luminosity is approximately linearly proportional to the disk mass M_d and temperature $T_0 r_0^q$, and depends weakly on the choice of outer radius R_d and the density exponent p. The choice of inner radius r_0 is unimportant. Thus, only five parameters, M_d, R_d, κ_ν, q, and $T_0 r_0^q$, are significant for determining the emission, and two of these, q and $T_0 r_0^q$, are established from infrared spectra where the emission is optically thick. Only R_d and κ_ν are poorly constrained from this dataset, although in principle R_d can be established from observations of the turnover frequency ν_d. Millimeter wavelength observations then determine the product $\kappa_\nu M_d$.

Optically thick emission cannot be completely neglected, even at very long wavelengths. As seen in Eq. (18), emission is dominated by the radii near r_1. The ratio of optically thick to optically thin emission referred to in Eq. (17) is given exactly by

$$\Delta = \frac{1}{\tau_0 r_0^p} \frac{2-p-q}{2-q} \frac{r_1^{2-q} - r_0^{2-q}}{R_d^{2-p-q} - r_1^{2-p-q}}$$

$$\approx -\frac{p}{(2-q)\ln\{[(2-p)/2]\bar{\tau}\}}. \tag{20}$$

The logarithmic dependence is strictly true only when $2 - p - q = 0$. Whenever $2 - p - q$ is small, however, Δ is a weak function of disk parameters. Because of the nearly logarithmic dependence, there is almost always some contribution from the optically thick region to the long-wavelength emission. Nevertheless, since Δ will be less than one for almost all objects in this survey, the correction factor $(1 + \Delta)$ is modest, and rather well determined from the observations.

By differentiating L_ν with respect to frequency, we can determine the spectral index α, defined as

$$\alpha = \frac{d(\log L_\nu)}{d(\log \nu)} = \frac{\nu}{L_\nu}\frac{dL_\nu}{d\nu}. \quad (21)$$

Expressing κ_ν as a power law in frequency with index β and using Eq. (17) allows us to express α approximately as

$$\alpha \approx 3 + [\beta/(1+\Delta)]. \quad (22)$$

For a disk that is optically thick, Δ is large, and $\alpha \approx 3$, as it should be for the sum of blackbodies in the Rayleigh–Jeans limit. If the disk is optically thin, Δ is small, and $\alpha \approx 3+\beta$, so that the power law index of the particle emissivity modifies the spectral index directly. Since Δ depends logarithmically on M_d and R_d, it can be determined fairly well, even if M_d and R_d are only loosely constrained from spectral fits to the data.

e) Millimeter-Wave Mass Opacity

Choice of the mass opacity κ_ν creates the largest uncertainty in the derivation of disk masses from the 1.3 mm flux densities. Recent estimates of κ_ν in the literature span a range of a factor of 30, from 0.002 to 0.10 cm^2 g^{-1} (Draine 1989). Most determinations are compatible at a wavelength of 30 μm; the divergence comes about from differences in the assumed frequency dependence of κ_ν at longer wavelengths.

Observational determinations of the mass opacity require several steps and assumptions, each of which introduce uncertainties into the final result (cf. Hildebrand 1983). A further complication is the probability that grains differ in the diffuse interstellar medium, dense interstellar clouds, and circumstellar disks. Part of the variation in determinations of κ_ν can be attributed to the differing environments of grains studied by various authors.

Unfortunately, even theoretically calculated values can differ by large factors, owing to the unknown *shape* of a typical grain: Draine and Lee (1984) calculate κ_ν (1.3 mm) ≈ 0.002 cm^2 g^{-1} for mixtures of silicate and graphite spheroids; Wright (1987) shows κ_ν may be increased by a factor of 30 or more if the grains are open structures of fractal dimension. The frequency dependence of κ_ν is quite different for the two particle types: small spheroids of silicate or graphite will have indices $\beta = 2$ longward of about 100 μm, owing entirely to the variation in the complex index of refraction; fractal particles may have $\beta \lesssim 1$ even beyond 1 mm. In principle, particle types might be distinguished by the frequency dependence of the opacity at very long wavelengths.

Spectral indices at 1 mm are available for four stars in the sample. Table III presents the flux densities at 2.7 and 1.3 mm, the calculated spectral index α, defined in Eq. (21), and the estimated value of β from Eq. (22) and our estimates of Δ discussed in the next section. If the millimeter-wave emission is primarily optically thin ($\Delta < 1$), all of these stars require $\beta \lesssim 1$ for adequate fits to the spectral index between 1.3 and 2.7 mm. The 2.7 mm continuum flux densities from T Tau and DG Tau may include contributions from free–free emission, which should make $\beta \gtrsim 0$, but will not make $\beta \sim 2$.

Alternatively, if the disks are optically thick even at millimeter wavelengths, the spectral indices will be insensitive to β. This would be the case for relatively massive, compact disks. The minimum mass and radius needed to fit HL Tau using $\beta = 2$ and Hildebrand's (1983) normalization are $0.9\mathcal{M}_\odot$ and 50 AU. For GG Tau, a $1.6\mathcal{M}_\odot$ disk with radius of 70 AU provides an adequate fit to the spectrum. But both of these disks would be more massive than their central stars and probably unstable to gravitational perturbations.

We may estimate an upper bound on the disk mass for HL Tau by making use of the gas orbital velocities a few hundred AU from the star. Sargent and Beckwith (1987) demonstrate that the total mass of the star plus disk is between 0.5 and 1 $\mathcal{M}_\odot$, based on the rotation curve of ^{13}CO. Table II gives the mass of the star as $0.55\mathcal{M}_\odot$, putting an upper bound of $0.5\mathcal{M}_\odot$ for the disk alone. This is about one-half the value required to make the disk optically thick at 1 mm. As described in the next section, the mass of the disk derived from the millimeter-wave and far-infrared flux densities is 0.1 (0.02 cm^2 g^{-1}/κ_ν) $\mathcal{M}_\odot$, where κ_ν is the mass opacity at 1.3 mm. Therefore, a lower bound to κ_ν is 0.004 cm^2 g^{-1}, a value close to that implied by Hildebrand's (1983) relation using $\beta = 2$ to extrapolate from the determined value at 250 μm. It is two times greater than that advocated by Draine and Lee (1984) for ISM, the value adopted by ALS in their disk models.

Perforce, the calculations of Draine and Lee (1984) are inadequate for these disks. Moreover, the long-wavelength emissivity dependence favored by Hildebrand (1983) does not properly describe some of the spectral indices presented in Table III. Grain growth in the dense disks is likely, and it should not be surprising that particle emissivities can be enhanced over those attributed to small particles in the ISM. The question becomes: what value of κ_ν most accurately described the particle properties in these disks?

If grain growth is spheroidal, the emissivities and spectral indices will be indepedent of grain size (Hildebrand 1983). If the grain growth leads to fractals, as suggested by Wright (1987) and others, the emissivities will be enhanced and the spectral indices decreased. To accommodate the uncertainties in this process, we adopted the general form $\kappa_\nu = 0.1(\nu/10^{12}\ \mathrm{Hz})^\beta$ cm^2 g^{-1}, with $\beta = 1$, giving $\kappa_\nu = 0.02$ cm^2 g^{-1} at 1.3 mm to apply to all the objects in our sample. This form is identical to Hildebrand's for $\lambda \lesssim 250$ μm, and for $\lambda \gtrsim 250$ μm is approximately the geometrical mean between the lower bound derived above and the largest opacities in the literature. This choice allows for a factor of 5 uncertainty in either direction, encompassing the values for κ_ν determined observationally and the most recent estimates of opacity enhancement owing to nonspherical coagulation.

TABLE III. Spectral indices.

HBC	Object	F_ν (1.2 mm)	F_ν (2.7 mm)	α	β
35	T Tau	280 ± 9	75 ± 15[a]	2.8 ± 0.3	-0.3 ± 0.4
37	DG Tau	443 ± 20	95 ± 15[b]	3.1 ± 0.3	0.2 ± 0.4
49	HL Tau	879 ± 19	120 ± 15[c]	3.7 ± 0.1	1.1 ± 0.2
54	GG Tau	593 ± 53	80 ± 5[b]	3.7 ± 0.2	1.6 ± 0.4

F_ν's are in mJy; α and β as defined in Sec. IV*d*.
[a] Wientraub, Masson, and Zuckerman (1987).
[b] Sargent and Beckwith (1989).
[c] Sargent and Beckwith (1990).

As seen in the next section, it implies the disk masses are comfortably less than the stellar masses, on average, and gravitational instabilities need not limit the disk lifetimes.

f) Properties of Disks

Infrared spectral energy distributions for many of our objects are presented by Strom *et al.* (1989) and spectra of additional stars may be obtained from the *IRAS Point Source Catalogue*. Power law fits to the infrared spectra between wavelengths of approximately 10 and 100 μm determined q and $T_0 r_0^q$ following Eq. (10). A single power law for the temperature distribution of the disk provides good fits to the spectral energy distributions at long wavelengths, but at short wavelengths heating by the star—often called *reprocessing*—will modify the index q. Although unimportant for the 1.3 mm observations, we included this heating according to the prescription of ALS to fit the short-wavelength data. The disk masses were calculated by numerically integrating Eq. (6) with $r_0 = 0.01$ AU, $R_d = 100$ AU, $p = 1.5$, and $\theta = 0$ to obtain the best fit to L_ν at 1.3 mm.

Figure 2 shows the observed and calculated spectral energy distributions of eight stars representative of the sample. The solid lines are fits using Eq. (6) with the disk extending to the stellar surface. The dashed lines show the modification for disks that have been cleared of material out to several stellar radii (r_0 was in the range 0.02–0.3 AU). The dotted lines are fits to the stellar photosphere using only a Planck function at the effective temperatures. All spectra have been dereddened using A_V from Table II. The figure includes six stars with energy distributions easily fit by the calculations, typical of the majority of the sample, and two stars that are extreme cases. The disk radiation in HL Tau completely dominates that from the star; several of the stars with high disk temperatures ($T_1 \gtrsim 300$ K) are similar, e.g., DG Tau, Elias 1, and RY Tau). It was difficult to simultaneously fit the far-infrared and millimeter-wave data for CY Tau; this star is discussed in more detail below.

The fits are good for most of the stars in the sample. The temperature of the disk at any radius is well constrained by the strength of the infrared emission. The disk particles are

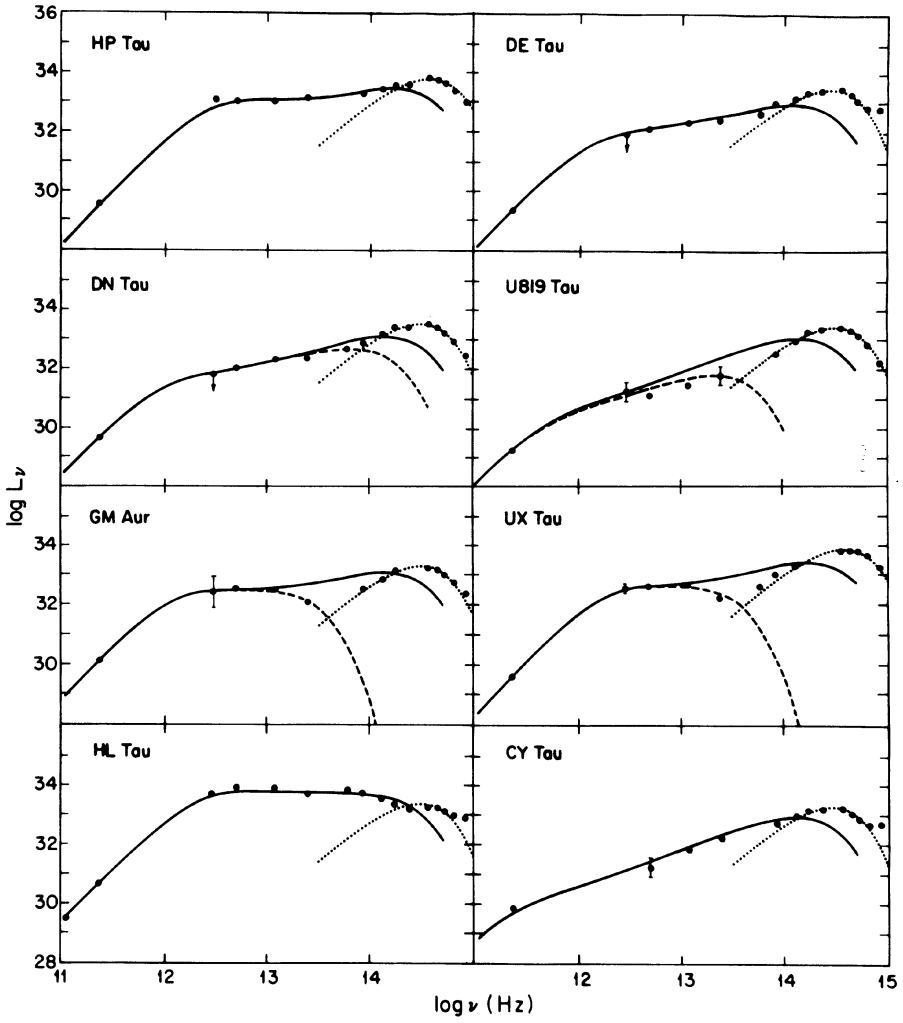

FIG. 2. Spectral energy distributions of eight stars in the sample. The ordinates are log (L_ν) as defined in the text. The solid lines are calculations of the disk radiation for disks extending from the stellar surface to R_d, normally 100 AU. The dashed lines are calculated spectra for disks that are clear of material from the stellar surface to an inner radius r_0, usually between 0.1 and 0.3 AU. The dotted lines are Planck functions at the stellar effective temperatures fitted to the short-wavelength data. The data at frequencies greater than 10^{14} Hz are corrected for extinction using the values in Table II.

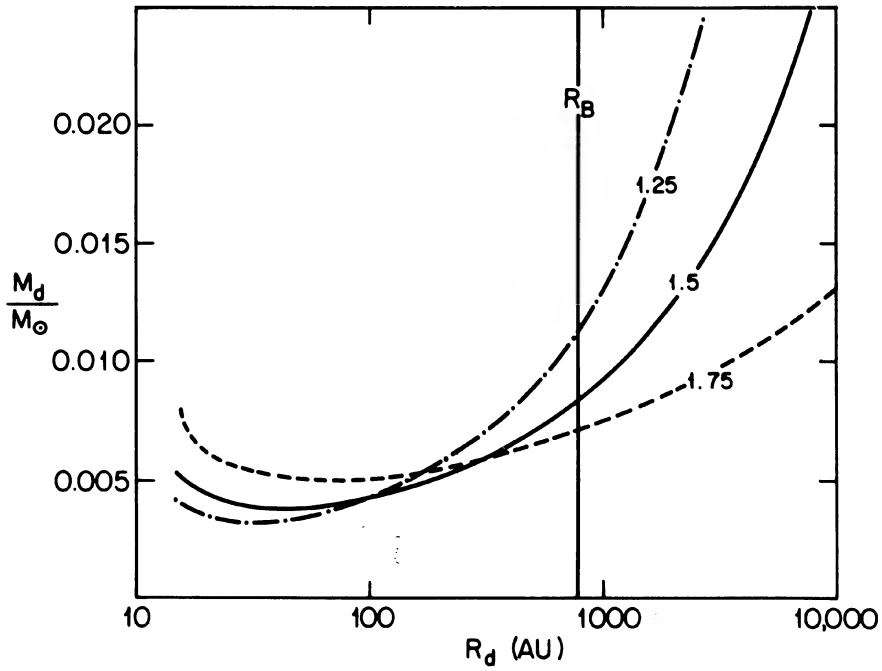

FIG. 3. Derived disk mass M_d as a functin of assumed disk radius R_d shows the relatively weak dependence of M_d on R_d in the numerical calculations. Three different values of the density exponent are shown: $p = 1.25$ (dot-dash); $p = 1.5$ (solid); $p = 1.75$ (dashed). The vertical line at $R_d = 750$ AU is the beam radius at 140 pc.

generally warmer than 100 K at 1 AU from the stars. The major uncertainty in the disk masses are in our choice of κ_ν at 1.3 mm.

In the majority of cases, the masses are insensitive to exact choices of q, T_1, and θ. In no case does the choice of r_0 affect the derived mass. We intend to discuss in detail the uncertainties in the multiparameter fits in a future paper, but we note that in almost all cases, plausible variations of q and T_1—maintaining consistency with the spectral energy distributions—and θ led to variations in the derived mass of 50% or less. These uncertainties are less than those introduced by unknown κ_ν and R_d. A few exceptions are discussed below.

Because R_d, the outer radius of the disk, is unknown for these stars, it is useful to compare mass estimates for different values of R_d and density distribution. Figure 3 is a plot of disk mass of HP Tau versus assumed R_d for three different values of the surface density power law index p. The value of R_d, in fact, affects the derived mass weakly over the range $20 \lesssim R_d \lesssim 300$ AU; the $R_d^{0.5}$ dependence indicated by Eq. (19) becomes important only for $R_d \gtrsim 500$ AU, where the disk optical depth becomes small enough to make the approximations valid. The lower bound to R_d is required for the disk to produce the observed 1.3 mm emission in the optically thick case. Since the beam radius (5.5″) limits the observed disk radii to 770 AU, the derived disk masses are probably accurate to better than a factor of 2 regardless of the actual values of R_d. Choosing $R_d = 100$ AU also makes the results insensitive to the density distribution (cf. Fig. 3).

Table IV lists the results of this fitting procedure in the cases where infrared data are available. Columns 3 and 4 give q, the temperature power law index, and T_1, the disk temperature at 1 AU; italicized object names indicate uncertain infrared flux densities and correspondingly uncertain fits for q and T_1. The disk masses appear in column 5. Column 6 lists r_1 in AU, and column 7 shows the fraction Δ of the 1.3 mm flux density contributed by optically thick emission. The *calculated* disk luminosity L_d appears in column 8. This luminosity depends fairly strongly on the choice of inner radius, but we list it here for comparison for the stellar luminosities. For these stars with only upper limits at 1.3 mm, the calculated luminosity is an upper limit.

A few stars required different choices of R_d or q to produce satisfactory fits. The far-infrared spectrum of CY Tau is best fitted with $q = 0.69$; however, this value of q is too large to produce the observed 1.3 mm flux density, even in the optically thick case. We chose $q = 0.68$, which fits the far-infrared spectrum within the uncertainties and gives a good fit to the 1.3 mm datum. The derived disk mass is extremely sensitive to the choice of q for this star—it is the only star in the sample for which this is true—because the 1.3 mm flux density is large in comparison with the infrared. With $q = 0.68$, the derived mass is also sensitive to the choice of disk radius. A disk radius of 150 AU was used for the derived mass. In any case, the mass is uncertain because the disk is optically thick at 1.3 mm ($\Delta = 6$).

For the stars HP Tau and SU Aur, $\beta > 1$ gives a better fit to the 100 μm and 1.3 mm flux densities; however, the 100 μm flux densities are difficult to accurately determine, especially because the spatial resolution of the *IRAS* observations is poor, allowing contamination by diffuse emission from regions beyond the disks. No other millimeter or submillimeter observations were available to determine β.

An outer disk radius of 20 AU gave a simultaneously good fit to the 100 μm and 1.3 mm data for the star RY Tau. The derived mass is not too sensitive to this choice, so long as $R_d \geqslant 20$ AU. A plot of M_d vs R_d for RY Tau is very similar to that for HP Tau shown in Fig. 3. As can be seen in the figure, the derived mass becomes large only for $R_d \leqslant 14$ AU.

TABLE IV. Disk properties

HBC	Object	q	T_1	M_d	r_1	Δ	L_d
24	FN Tau	0.54	156	0.004	3	0.2	0.3
28	CY Tau	0.68	79	0.7[b]	88	6	0.12
33	DE Tau	0.57	133	0.007	4	0.3	0.3
34	RY Tau[d]	0.51	360	0.039	20	6	11
35	T Tau	0.51	390	0.016	7	0.3	17
37	DG Tau	0.51	308	0.041	15	0.4	8
41	IQ Tau	0.64	128	0.040	15	0.6	0.4
43	UX Tau A[c]	0.52	169	0.009	5	0.3	0.3
45	DK Tau	0.62	188	0.005	3	0.3	2
48	HK Tau[c]	0.46	150	0.005	3	0.2	0.3
49	HL Tau	0.49	307	0.10	25	0.5	6.7
51	V710 Tau	0.64	112	0.038	12	0.6	0.3
52	UZ Tau	0.62	173	0.054	14	0.5	1.4
54	GG Tau	0.55	180	0.29	45	1.2	0.9
58	DL Tau	0.59	158	0.087	24	0.7	0.7
61	CI Tau	0.58	156	0.063	20	0.6	0.6
62	DM Tau[c]	0.51	108	0.034	13	0.4	0.06
63	AA Tau	0.55	135	0.021	9	0.4	0.3
65	DN Tau	0.58	123	0.027	11	0.5	0.3
66	HP Tau	0.50	203	0.005	4	0.2	1.2
67	DO Tau	0.54	203	0.018	9	0.3	1.4
70	DP Tau	0.61	144	0.003	2	0.3	0.6
71	GO Tau	0.60	93	0.057	17	0.7	0.1
72	DQ Tau	0.59	141	0.025	9	0.4	0.5
74	DR Tau	0.62	227	0.028	11	0.5	4.
75	DS Tau	0.66	100	0.010	6	0.5	0.2
76	UY Aur	0.55	243	0.004	2	0.2	2.0
77	GM Aur[c]	0.51	152	0.060	19	0.5	0.2
367	V773 Tau	0.75	207	0.010	6	0.5	1.3
373	Elias 1	0.49	388	0.013	7	0.2	16
378	V819 Tau	0.65	68	0.032	13	0.8	0.06
384	FT Tau	0.55	139	0.034	13	0.4	0.3
396	Haro 6-13[c]	0.54	200	0.014	5	0.2	0.8
401	FY Tau	0.70	156	0.003	2	0.4	0.6
402	FZ Tau	0.66	152	0.004	3	0.3	0.5
429	*V836 Tau*	0.63	90	0.010	3	0.4	0.10
	Haro 6-39	0.53	103	0.005	4	0.3	0.08
23	FM Tau	0.55	140	<0.005	3	0.2	0.3
25	CW Tau	0.59	199	<0.015	7	0.3	1.8
26	FP Tau	0.60	94	<0.025	< 9	< 0.5	0.1
27	CX Tau	0.57	109	<0.011	< 6	< 0.3	0.13
29	V410 Tau						
30	DD Tau[c]	0.54	200	<0.005	< 4	< 0.2	0.4

T_1 is in K; M_d is in $M_\odot$; r_1 is in AU; and L_d is in $L_\odot$. Italics indicate far infrared flux densities, q, and T_1 are uncertain.

[a] Best fit was 0.69; forced to 0.68 to fit F_ν(1.3 mm).

[b] R_d = 150 AU assumed.

[c] Low near IR flux densities; $0.05 \lesssim r_0 \lesssim 0.3$ AU.

[d] R_d = 20 AU necessary for good fit to 100 μm flux.

TABLE IV. (continued)

HBC	Object	q	T_1	M_d	r_1	Δ	L_d
31	*CZ Tau*[e]	0.49	171	<0.003	< 2	< 0.2	0.5
32	BP Tau	0.62	119	<0.011	< 6	< 0.4	0.3
36	DF Tau	0.75	130	<0.010	< 4	< 0.5	2.3
38	DH Tau	0.55	103	<0.017	< 8	< 0.4	0.1
39	DI Tau	0.54	90	<0.011	< 6	< 0.3	0.05
44	FX Tau	0.63	118	<0.005	< 4	< 0.3	0.3
46	*ZZ Tau*	0.69	68	<0.014	< 7	< 0.7	0.08
47	V927 Tau	0.56	63	<0.012	< 6	< 0.4	0.01
50	XZ Tau	0.51	233	<0.001	< 1	< 0.2	2.0
55	GH Tau	0.61	140	<0.006	< 4	< 0.3	0.5
56	GI Tau	0.60	160	<0.003	< 2	< 0.2	0.5
57	GK Tau	0.72	155	<0.003	14	< 0.1	0.7
59	IS Tau	0.75	80	<0.023	< 10	< 1	0.3
60	HN Tau	0.68	163	<0.006	< 4	< 0.4	0.7
64	HO Tau	0.62	80	<0.019	< 9	< 0.5	0.06
68	VY Tau	0.52	97	<0.015	< 7	< 0.3	0.06
69	V995 Tau	0.56	150	<0.009	< 5	< 0.3	0.5
79	SU Aur	0.51	259	<0.003	1	< 0.2	3.1
369	FO Tau	0.62	121	<0.017	8	< 0.4	0.3
374	Hubble 4						
377	*FQ Tau*	0.59	77	<0.026	10	0.5	0.04
383	FS Tau	0.52	205	<0.003	< 2	< 0.2	1.3
386	FV Tau	0.58	189	<0.004	< 3	< 0.3	1.4
399	*V827 Tau*	0.55	72	<0.015	8	< 0.4	0.02
400	*V826 Tau*	0.61	67	<0.022	10	< 0.6	0.03
405	*V830 Tau*	0.56	75	<0.022	10	< 0.5	0.03
409	*FF Tau*	0.60	63	<0.024	< 9	< 0.6	0.02
416	Haro 6-28						
418	HV Tau						
420	*IW Tau*	0.60	69	<0.069	11	< 0.5	0.03
	FR Tau						
	FU Tau	0.50	97	<0.008	< 5	< 0.3	0.07
	GT Tau						
	FW Tau	0.74	56	<0.046	16	< 2	0.07
	ZZ Tau B						
	IT Tau	0.63	103	<0.006	< 4	< 0.4	0.18
	HQ Tau	0.69	168	<0.011	6	< 0.4	0.8
	FG Tau	0.52	75	<0.021	< 8	< 0.4	0.02
	HD 283759	0.46	103	<0.006	< 4	< 0.2	0.07
	FI Tau	0.53	78	<0.023	10	< 0.4	0.03
	HT Tau	0.61	76	<0.046	16	< 0.7	0.04
	GN Tau	0.63	126	<0.016	8	< 0.5	0.4
	Haro 6-32						

[e] L_d exceeds apparent L_{bol} at short wavelengths.

[f] Calculated far-infrared flux density too high for longest wavelength.

[g] $\beta = 1.5$ used for best fit to 100 μm and 1.3 mm data.

[h] $\beta = 0$ used for best fit to 60 μm, 100 μm, and 1.3 mm data.

Five close pairs make the IRAS-determined far infrared fluxes uncertain because of beam confusion: DD & CZ Tau, DH & DI Tau, HL & XZ Tau, GH & GK Tau, and FY & FZ Tau. The corresponding q's and T_1's are uncertain.

The spectra of DD Tau, T Tau, HL Tau, UX Tau, DM Tau, GM Aur, and Haro 6-13 have lower 12 μm flux densities than expected for disks that extend into stellar surface. More generally, many of the stars in the sample have near-infrared (3–12 μm) emission smaller than expected from disks extending into the stellar surfaces that simply reprocess the star's luminosity (cf. ALS). The results *require* the inner regions of the disks to be optically thin and essentially clear of material. These are noted in Table IV as stars requiring the inner radius r_0 to be greater than 0.05 AU for adequate fits to the near-infrared data. In all cases, an inner disk radius between 0.05 and 0.3 AU produces an adequate fit to the energy distributions. High inclination angles of some disks will lead to an uncertainty in the temperature scale T_1. If so, the temperature estimates for the disks will be low by a factor of $(\cos\theta)^{q/2}$ [Eq. (10)], and the mass estimates will be too high by a corresponding factor. Since $q \sim 0.5$, the error is a factor of 2 or more only for $\theta \gtrsim 86°$. Uncertainties introduced into the mass estimates by the unknown disk inclinations will, in general, be smaller than the other uncertainties, particularly in κ_ν.

The division of the far-infrared flux between close pairs—DD and CZ Tau, DH and DI Tau, HL and XZ Tau, GH and GK Tau, and FY and FZ Tau—is uncertain, owing to the close proximity of the stars and the relatively large *IRAS* beam. For example, SSECS attribute considerably more far-infrared emission to XZ Tau than we would guess from the relatively low 1.3 mm emission. The assumed division affects the XZ Tau mass strongly and the HL Tau mass weakly. Since XZ Tau gave only an upper limit at 1.3 mm, there is no clear basis for assigning its far-infrared flux densities more accurately. We caution that the disk properties derived from the assumed far-infrared flux—q, T_1 and L_d—are probably in error.

For the more massive disks, a substantial fraction of the millimeter continuum emission is optically thick, as seen by the values of Δ in Table IV. This runs counter to accepted wisdom that very long-wavelength thermal radiation comes from transparent regions and underscores the high surface densities in the inner parts of the disks. The increased size of the optically thick part decreases the spectral index relative to that expected for a completely transparent disk. The effect is pronounced for the massive disks such as HL Tau, and means it will be difficult to determine β from *submillimeter* observations because of the large correction factor in Eq. (22). Several of the stars discussed by Weintraub, Sandell, and Duncan (1989) have this problem.

Disk temperatures resulting from these fits are closely correlated with the 60 μm flux density. Figure 4 shows the derived 1 AU disk temperatures versus F_ν(60 μm), the 60 μm flux density. The tight correlation demonstrates that the far-infrared flux is essentially a measure of disk temperature, the other disk properties being largely irrelevant. The disk masses are similarly correlated with the 1.3 mm flux density, although the correlation is not as tight because temperature and mass affect the 1.3 mm flux density equally. The derived disk mass is plotted against F_ν(1.3 mm) in Fig. 5. The scatter is largely due to temperature uncertainties and emphasizes the need for good infrared fluxes to obtain accurate disk masses from the long-wavelength data.

The average disk mass is a few percent of a solar mass, depending on κ_ν and the underlying distribution at the low-mass end. Most disks are only a few percent of the stellar mass. Figure 6 shows the distribution of disk masses for those objects detected in the survey. The upper part is a histogram of log M_d; the lower part is the underlying probability distribution calculated from the maximum-likelihood method presented by Avni *et al.* (1980), a general application of the Kaplan–Meier estimator. The most massive disks, GG Tau and HL Tau, are still smaller than their parent stars (the CY Tau result is quite uncertain). Even if the masses were increased by a factor of 5 to accommodate a different value for κ_ν, only a few of the disks would be more massive than their central stars.

Disk temperatures exhibit a wide range, from a few tens of degrees to a few hundred degrees. The distribution of T_1, shown in Fig. 7, indicates an average temperature near 120 K. The central stars are usually more luminous than $1L_\odot$, and so the typical disk temperature is *smaller* than the equilibrium temperature for small particles exposed to the radiation from the star at 1AU. This is probably true for even the hot disks, although there is considerable uncertainty in the

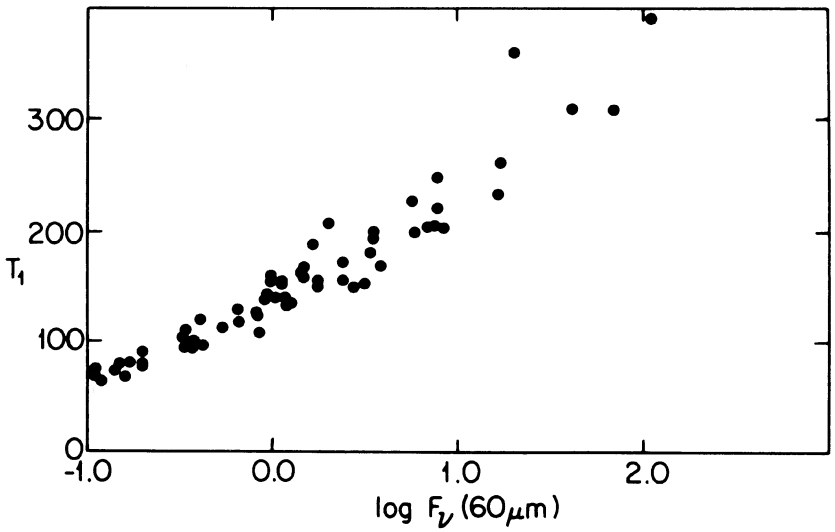

FIG. 4. Disk temperature at 1 AU, T_1 derived from the spectral fits is plotted vs the logarithm of the flux density at 60 μm. The very tight correlation shows that T_1 is well determined from the far-infrared observations, with other parameters—notably the temperature index q—having little effect.

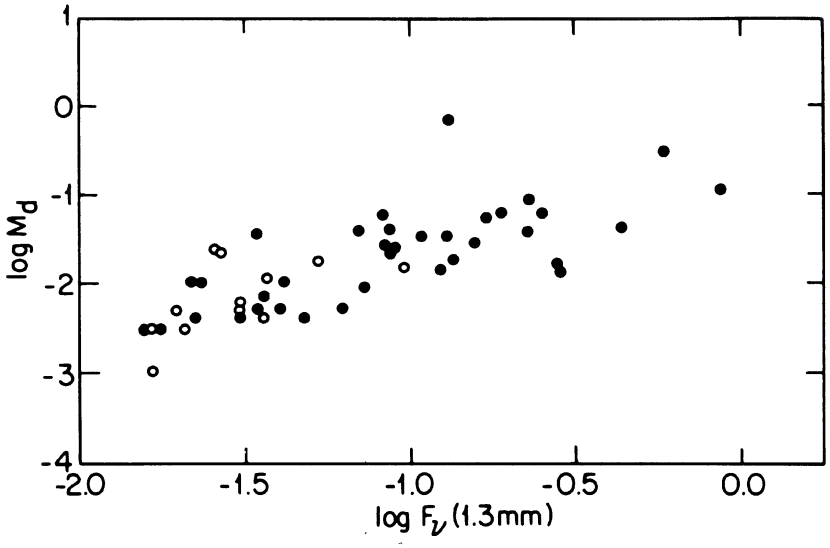

FIG. 5. Logarithm of derived disk mass M_d vs the 1.3 mm flux density F_ν shows the correlation of F_ν with total amount of emitting material; the scatter indicates variation in the disk temperatures that must be taken into account for an accurate derivation of M_d.

stellar luminosity owing to the unknown contribution from the disk. Disks with the lowest temperatures are often colder than they should be from heating by the star alone, at least at radii less than 1 AU from the stars. V819 Tau is a good example. These stars must also have optically thin inner regions resulting in a deficit of infrared emission.

Many of the disks have temperature indices q close to 0.5, the "flat-spectrum" sources of ALS. The distribution of q appears in Fig. 8. Almost none of the disks have indices as large as 0.75, the value for a pure accretion disk or a thin disk that reprocesses luminosity from the central star. *All* disks with temperatures $\gtrsim 200$ K have flat spectra ($q \sim 0.5$). Figure 9 is a plot of the temperature index q against the temperature T_1. Only low-temperature disks have $q \gtrsim 0.6$, and these disks have the most uncertain fits owing to the small infrared flux densities. There is a weak anticorrelation between q and T_1: q tends to decrease as T_1 increases. It is particularly noteworthy that there are *no* disks with q much less than 0.5.

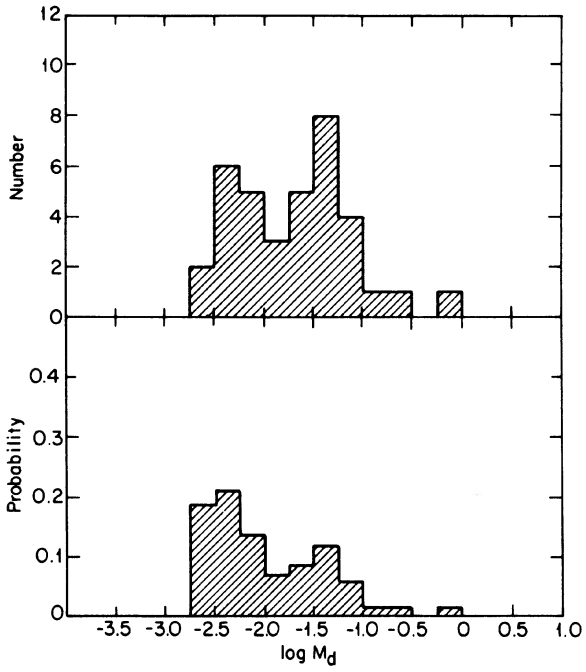

FIG. 6. Distribution of disk masses for the 37 stars detected at 1.3 mm. The upper part of the figure is the histogram of disk masses from Table IV. The lower part of the figure shows the underlying probability distribution calculated from a maximum-likelihood method described in the text.

V. DISCUSSION

a) Disk Characteristics and Evolutionary Trends

Almost half the objects in the sample were detected at 1.3 mm. We have argued that this emission arises in circumstellar disks. Disks are clearly prevalent among pre-main-sequence stars that have masses between 0.2 and 2 $\mathcal{M}_\odot$. Their preponderance has also been noted by other authors using far-infrared spectra as indicators (Strom *et al.* 1986, 1989; Cohen, Emerson, and Beichman 1989). Since our survey is

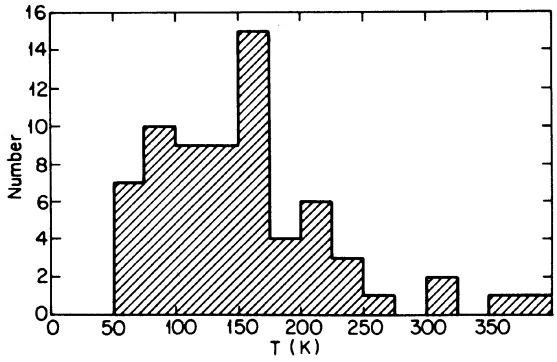

FIG. 7. Distribution of disk temperatures at 1 AU for the stars with known infrared flux densities.

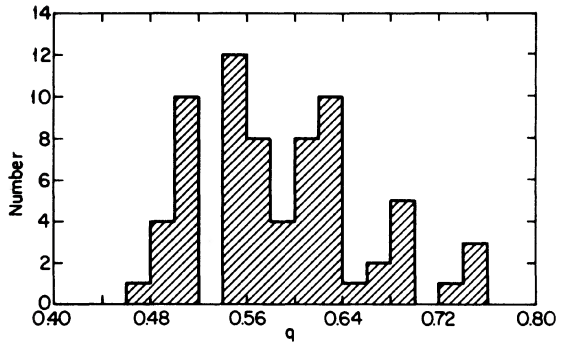

FIG. 8. Distribution of temperature power law indices q. It is noteworthy that none of the stars has q significantly less than 0.5, and only three stars have an index $q \approx 0.75$ expected for a pure accretion or reprocessing disk.

sensitive to disk mass and, owing to the small beamsize, suffers less from confusion due to extended cloud emission or Galactic cirrus, it provides a more statistically reliable sample of detections. Nonetheless, the fraction of detected objects is almost identical to far-infrared surveys.

Disk masses range from approximately 0.001 to 0.5 $\mathcal{M}_\odot$, the lower limit set by the sensitivity of our observations and the upper value being uncertain, depending strongly on the choice of unknown disk parameter to fit the spectra. The average mass, $\sim 0.02 \mathcal{M}_\odot$, is similar to that assumed for the early solar nebula. These masses refer to hydrogen gas, which is assumed to be 100 times the particle mass actually detected at 1.3 mm. As described in Sec. IV, the principal uncertainty in disk mass is the choice of 1.3 mm opacity per unit mass κ_ν. We chose a larger value for κ_ν than usually assumed for interstellar dust particles, so that the disk masses may be larger than those derived here. There is certainly enough material to form planets around most of these stars. Although a variety of precesses may conspire to dissipate these disks on timescales comparable to those required for planet formation (Wolstencroft and Walker 1988; Backman, Gillet, and Witteborn 1989), we see little evidence of this in our sample (see below). We are further encouraged by the fact that evidence for residual disks of much lower mass has been found for almost 50% of a sample of nearby main-sequence A stars (Backman and Gillet 1987) to believe that planetary systems should be relatively common in the Galaxy.

On the other hand, almost all the disks are much less massive than their central stars, usually by more than a factor of 10. ALS supposed that typical disks for the flat-spectrum sources were fairly massive, $1 \mathcal{M}_\odot$, or more, based largely on the small value for κ_ν favored by Draine and Lee (1984). It is clear from the spectral indices that the long-wavelength opacity does not conform to the Draine and Lee model; our millimeter-wave results indicate significantly less mass, at least at radii beyond $r_1 \sim 1$ AU where the emission is optically thin. Our parametrization of the surface density, $\Sigma \propto r^{-1.5}$, assumes most of the mass is at large radii, and the mass in the optically thick portion at small radii is a small fraction of the total. Only if the surface densities are such steep functions of radius that most of the mass is concentrated near the star would the millimeter observations be insensitive to the bulk of the material, a situation we regard as unlikely. For the few cases where there are CO observations with very good spatial ($\lesssim 10''$) and velocity ($\lesssim 0.5$ km s^{-1}) resolution—HL Tau and DG Tau—disk masses of more than $\sim 0.5 \mathcal{M}_\odot$ are excluded by the rotation curves (Sargent and Beckwith 1987, 1989).

These disks are cold, in the sense that particles in radiative equilibrium with the central stars would be hotter than the disks at the same radii. Most disk particles are shielded from direct stellar radiation by high opacity within the disk. The temperatures are high enough to make the disk luminosity larger than the stellar luminosity in a few instances, however. In these cases, the disk luminosity is not driven by the stellar luminosity, unless the stellar luminosity has been grossly underestimated.

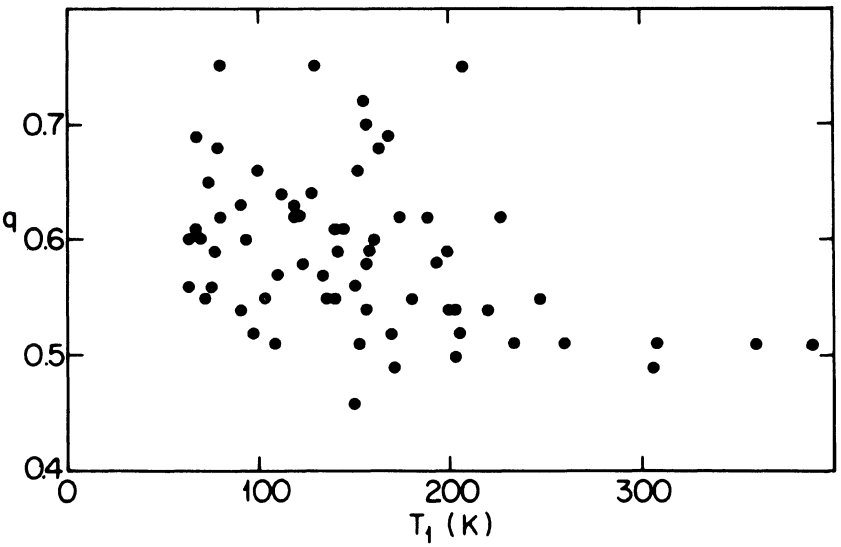

FIG. 9. Temperature index q plotted vs disk temperature T_1. All of the hottest disks have $q \sim 0.5$.

The particles in these disks appear to be different from the particles in the more diffuse interstellar medium. The four objects in this sample with well-determined spectral indices imply $\beta \lesssim 1$, if the emission is optically thin at 1.3 mm, whereas dust grains in molecular clouds typically have $\beta \sim 2$ (Hildebrand 1983; Emerson 1988). The smaller value for β might result because disk particles are larger than interstellar grains, perhaps the result of particle growth in the high-density environment of the disks. An attractive hypothesis is that grain growth is not spheroidal, but increases with fractal dimension, creating structures similar to interplanetary particles collected in the stratosphere (Millman 1975). Such structures couple well to long wave radiation, and their emissivities can easily be enhanced to give $\beta \lesssim 1$, even when the aggregate sizes are smaller than the wavelength (Wright 1987). A strong conclusion must await spectral index determinations for some of the more tenuous disks in the sample, where the optical depth must certainly be small.

We see little evidence for evolution of the disk mass over the 10^7 yr age span encompassed by this sample. Figure 10 displays the disk mass versus stellar age. There is no correlation between the two quantities up to the limiting age of the sample stars, approximately 10^7 yr. Evolution might be expected if, for example, disk matter dissipated as the disks evolved. The percentage of stars detected at 1.3 mm is not obviously a function of the stellar age, as can be seen by comparing the number of upper limits to detections in Fig. 10. Evidently, dissipation of material or condensation into very large particles ($\gg 1$ mm) takes longer than 10^7 yr in the outer parts of the disks ($r \gtrsim 1$ AU) to which this survey is sensitive. The most massive disks in the sample do not surround the youngest stars.

There is some evidence for disk temperature evolution, in the sense that older disks are colder, perhaps the result of diminishing energetic activity such as accretion or stellar luminosity. Figure 11 displays the temperature at 1 AU against the stellar age, showing a mild decrease of disk temperature in older stars. The decreasing temperatures weaken the far-infrared flux much more severely than do changes in disk mass. The older stars tend to be fainter at 1.3 mm for a given mass and also fainter at far-infrared wavelengths, an effect SSECS attribute to evolution of the disk masses. Decreasing temperature presumably reflects a decrease in energetic activity—from accretion, for example—among older disks. There may also be some tendency for clearing of the inner disk in these older stars, as indicated by the colder temperatures and less reprocessed radiation from the stars.

Several of the stars in the sample—V819 Tau, V826 Tau, V827 Tau, V830 Tau, and V836 Tau—are weak emission-line or "naked" T Tauri stars (Walter and Kuhi 1981; Feigelson and Kriss 1981). Walter (1987) and Walter *et al.* (1989) argue that the naked T Tauri stars are devoid of circumstellar matter, based on optical emission-line spectra and x-ray properties. V819 Tau has a fairly massive disk ($0.032 \mathcal{M}_\odot$), however, and V836 Tau was a marginal detection with a disk mass of order $0.01 \mathcal{M}_\odot$. The relatively small far-infrared fluxes from these objects means the disk *temperatures* are much lower than average, making it difficult to see the disk matter directly at any wavelength, but there is *no indication* from this sample that the naked T Tauri stars have *less* matter than other pre-main-sequence objects, at least in their outer parts.

Broadening the class of naked T Tauris to include those with very weak Hα lines, $\leqslant 10$ Å, SSECS concluded that many of these objects do have some circumstellar material, albeit less than the classical T Tauri stars. Figure 12 is a plot of disk mass versus Hα equivalent width WHα. There is an extremely weak correlation between disk mass and WHα, and a slight tendency for the objects with strong emission-line strength to have more massive disks. It is apparent from the figure that weakness of the emission lines does *not* imply the absence of disk material. The optical and x-ray properties of these stars are presumably a strong function of the high-energy phenomena, luminosity of the star/disk boundary layer, and generation of energetic mass outflow. It is a relatively weak function of the total amount of circumstellar material and we suggest that the optical and x-ray properties are inadequate to establish the presence or absence of a disk.

It is tempting to speculate that the stars with disks are isolated, whereas those without disks are members of multi-

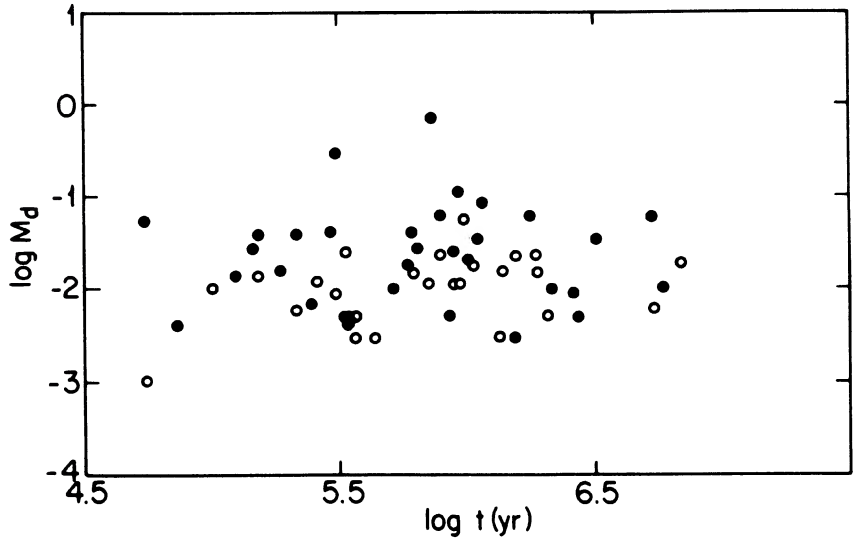

FIG. 10. Logarithm of disk mass is shown for stars of different age t. Solid circles are 1.3 mm detections; open circles with vertical lines are upper limits at 1.3 mm. There is no correlation between disk mass and stellar age, suggesting little evolution of the mass over the range 10^5–10^7 yr.

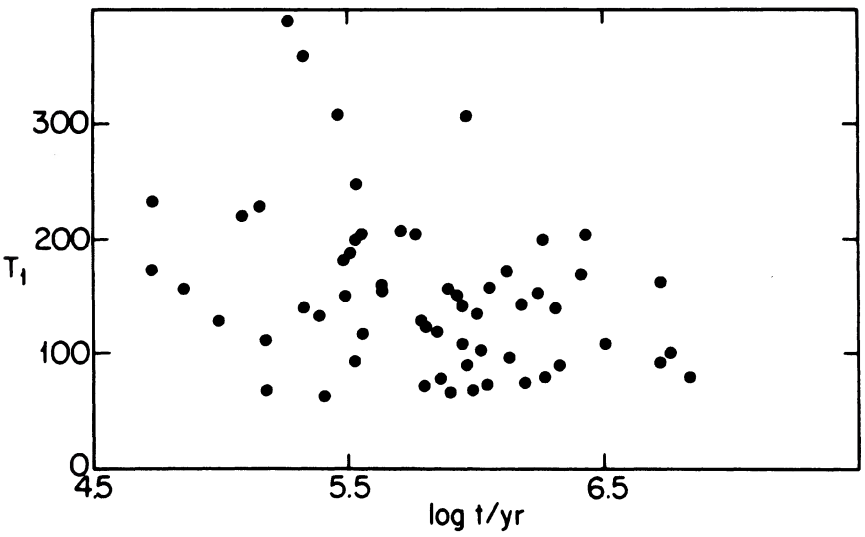

FIG. 11. Disk temperature T_1 is shown for stars of different age for all the sample stars with good infrared spectra. There is very little correlation between the temperature and age, although there is a tendency for the older stars to have cooler disks. If this trend is general, the older stars will be more difficult to detect at 1.3 mm, even if the disk masses are similar to those of the younger stars.

ple star systems. The excess angular momentum accompanying cloud collapse would be taken up either by a disk or a companion. Approximately 50% of all stars are isolated (Abt and Levy 1976), essentially the same fraction as those detected in this survey. Tidal forces from companions might inhibit disk formation.

The stars in this sample with close companions have very little disk mass. Table V lists the stars with known companions within the 10″ beam used for the 1.3 mm observations. Twelve stars have companions within 1″ (140 AU), and two more have companions within 3.5″ (500 AU). Only three of the 12 close binaries were detected at 1.3 mm, and two of these have very small masses, 0.004 and 0.009$\mathcal{M}_\odot$. T Tau has the most massive disk and probably the *least* massive companion. The two stars with more distant companions, V710 Tau and UZ Tau e, have average disk masses, 0.038 and 0.054$\mathcal{M}_\odot$, respectively. Pairs with separations comparable to or larger than the disk radii may have little effect on the disks. The upper limits to the disk masses for most of the other stars are small, typically less than 0.005$\mathcal{M}_\odot$.

Statistically, the presence of a close companion appears to inhibit the amount of material in a disk. If companions form with the stars, then tidal forces presumably limit the disk mass, perhaps through truncation of the outer parts or dissipation of the matter via tidal torques. Alternatively, companions may condense from disks. The results here then suggest that much of the disk material is used to make the companion stars before the companions become visible. Distant, low-mass companions, such as T Tau IR, may have little affect on the disks in their early stages.

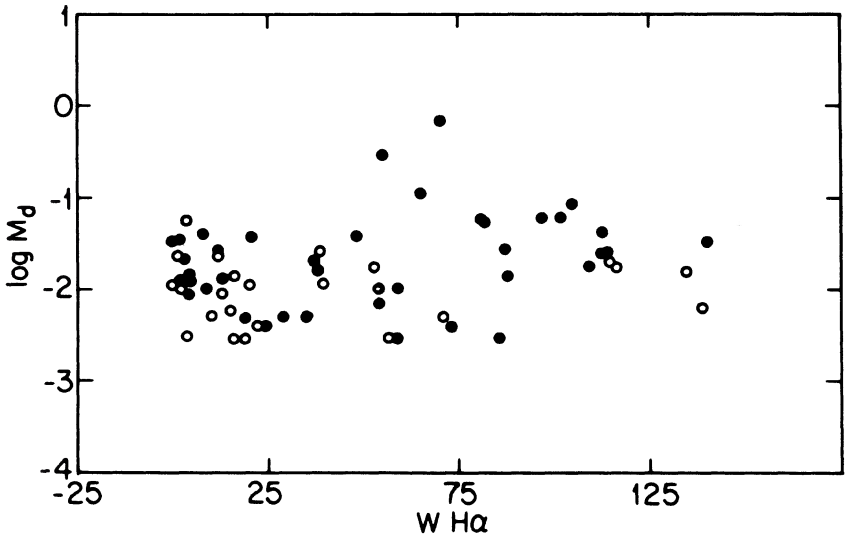

FIG. 12. Disk mass is shown vs Hα equivalent width to test the hypothesis that emission-line strength indicates presence or absence of a disk. There is at most a mild correlation suggesting more massive disks have stronger emission lines, but it is clear that even stars with little or no Hα emission have circumstellar disks.

TABLE V. Multiple star systems.

HBC	Object	δ (AU)	M_d	Ref
25	CW Tau	–	< 0.008	HHSM86
35	T Tau	75	0.013	DSZ82
36	DF Tau	10	< 0.006	CS88
39	DI Tau	72	< 0.011	CSLHB89
43	UX Tau	–	0.008	HHSM86
51	V710 Tau	500	0.018	CK79
52	UZ Tau e	500†	0.034	HHSM86
76	UY Aur	115	0.003	JVB44
383	FS Tau	< 60	< 0.002	CS89
386	FV Tau	88	< 0.003	CS88
400	V826 Tau	0.005	< 0.017	MWFFHO83
409	FF Tau	5	< 0.017	CS88
	FW Tau	118	< 0.046	CSLHB89
	HQ Tau	1.3	< 0.008	CS88

†UZ Tau e has an additional close companion, separation < 100 AU.

b) Disk Properties Related to Star and Planet Formation

A disk serves as the repository for almost all the angular momentum in an initially extended cloud as it collapses to form a star. The total angular momentum J_d for a disk may be calculated using the parametrization discussed in Sec. IV:

$$J_d = \int_{r_0}^{R_d} \sum(r) r v(r) 2\pi r\, dr \tag{23a}$$

$$\approx \frac{2-p}{2.5-p} M_d \sqrt{GM* R_d} \tag{23b}$$

$$\propto L_\nu \sqrt{GM*} R_d^{2.5-p}. \tag{23c}$$

The last line shows the explicit dependence on the observable quantities, L_ν and $M*$, as well as the unknown radius R_d. There is a rather strong dependence of J_d on R_d. We assume that R_d is 100 AU to an order of magnitude. Then, noting that $M* \sim 1\mathcal{M}_\odot$ and $M_d \sim 0.02\mathcal{M}_\odot$, a typical disk in this sample has an angular momentum $l_d \sim 6\times 10^{51}$ g cm^2 s^{-1}. The angular momentum contained in the Oort cloud of the solar system is $\sim 3\times 10^{51}$ g cm^2 s^{-1} (Marochnik, Mukhin, and Sagdeev 1988), within the uncertainties the same as the typical star in this sample. Since the large radii dominate J_d, and all of the matter at these radii is detected, it is unlikely that the actual angular momentum in the disks is more than a factor of 10 above this estimate.

On the other hand, this angular momentum could be much lower than that of the original clouds that collapsed to create the stars. Hartmann *et al.* (1986) estimate molecular cloud momenta, J_{MC} of order 10^{53}–10^{55} g cm^2 s^{-1} for the original protosolar nebula. And a $1\mathcal{M}_\odot$ star rotating near breakup velocity has an angular momentum $l* \sim \sqrt{GM^3* R}$. For $R* \sim 10^{12}$ cm, $l* \sim 2\times 10^{52}$ g cm^3 s^{-1}, although observations of T Tauri stars show they are almost always slowly rotating (Vogel and Kuhi 1981; Hartmann *et al.* 1986). The disks do *not* necessarily contain most of the angular momentum in the system. In fact, the typical disk in this sample has only a fraction of the angular momentum presumably contained in this initial cloud. We suppose only the low angular momentum parts of the collapsing cloud contribute to the star and disk.

The stored mechanical energy in the disks is negligible compared to that in the stars, and the timescale for radiating this energy is much shorter than the ages of the systems. Unlike the angular momentum, however, the disk kinetic energy is dominated by small radii:

$$E_d = \int_{r_0}^{R_d} \frac{1}{2}\Sigma(r) v^2(r) 2\pi r\, dr, \tag{24a}$$

$$\approx \frac{2-p}{2(p-1)} \frac{GM* M_d}{r_0} \left(\frac{R_d}{r_0}\right)^{p-2}, \tag{24b}$$

$$\propto L_\nu R_d^{2(p-2)}. \tag{24c}$$

Using (24b) with $M* \sim 1\mathcal{M}_\odot$, $M_d \sim 0.02\mathcal{M}_\odot$, and $R_d \sim 100$ AU, we can derive an upper limit to E_d using the stellar radius for r_0: $r_0 \gtrsim 10^{11}$ cm implies $E_d \lesssim 3\times 10^{44}$ ergs. The stored energy in the disk is tiny compared to that in the star, $GM^2*/r_0 \sim 10^{48}$ ergs, and it cannot provide for much of the disk luminosity. A characteristic time to deplete the stored energy is $t_d = E_d/L_d \sim 10^4$ yr, clearly much shorter than the lifetime of these disks. Therefore, it is clear that the energy source for the disk luminosity must be close to the star and transferred to the disk via radiation, magnetic fields, or gravity.

The energy transport must behave similarly to radiation in some essential characteristics. The distribution of spectral indices (Fig. 8) shows a preference for temperatures falling as $r^{-1/2}$, especially for the most luminous objects where the disk dominates the total luminosity (Fig. 9), and where the energy transport must be operating most efficiently. This dependence is identical to that followed by large particles in radiative equilibrium with a central luminosity source L where $T(r) = (L/16\pi\sigma r^2)^{0.25}$. The index -0.5 comes about because the flux decreases as r^{-2}, whereas the reradiated power is proportional to T^4. Any heating process that provides a heating flux falling with the inverse square of the distance will reproduce this law: The reason radiation fails for the thin disk is because the radial optical depth in the disk is so high that most distant particles cannot be heated directly by the star. And, as demonstrated in Sec. IV*c*, there is enough mass to make the radial optical depths prohibitively large, even if the matter were distributed isotropically around the star. It therefore appears likely that magnetic fields or gravity play the dominant role in heating the disks.

If accretion is ultimately responsible for much of the luminosity in these systems, the minimum accretion rates needed to generate that luminosity in the boundary layer near the stellar photosphere are large. For accretion luminosity L_a, the infall rate $\dot{M}$ is $2R*L_a/GM*$, which, for $M* \sim \mathcal{M}_\odot$, $R* \sim 10^{11}$ cm, and $L_a \sim L_\odot$ is $\sim 10^{-7}\,\mathcal{M}_\odot$ yr^{-1}. The disk mass, $0.02\mathcal{M}_\odot$, is replenished completely in less than 10^6 yr at this rate. The disks apparently persist longer than a few million years (Fig. 10), and unless most of the mass is hidden from view even at 1 mm, the large $\dot{M}$ suggests that material in at least the inner disk—$r \lesssim 1$ AU—must be transient; we are observing part of a continuous flow into the star. Philosophically, this is an unappealing circumstance; surely it would be easier to understand if the disks were the reservoir for all the mass. Given the uncertainties in these numbers, and especially the uncertainty in κ_ν, it is perhaps too early to conclude there is a real problem.

The actual thicknesses of the disks may be estimated from

the temperature and stellar mass. Writing the ratio of disk thickness H to the radius r as the ratio of sound speed to orbital velocity (Pringle 1981), $H/R \sim \sqrt{kTr/GM*\bar{m}} \sim 0.02$ at 1 AU for the typical disk. H/R increases no faster than $r^{0.25}$, in this approximation, so the disks are very thin out to several thousand AU. Very little of the stellar radiation or wind interacts with a typical disk, and the disks should be robust even for stars with large radiative and mechanical outputs. Therefore, the disk material should survive the T Tauri phase. The disks around the main-sequence stars, Vega and β Pictoris (Smith and Terrile 1984; Backman and Gillett 1987; and references therein) are orders of magnitude less massive than the average of our sample, and we consider condensation into large masses, such as plants, a likely possibility.

VI. CONCLUSIONS

Circumstellar disks commonly accompany the formation of solar mass stars; formally, we detected disks around 42% of a sample of 86 T Tauri stars in the Taurus dark cloud. The detected fraction is somewhat lower for stars with weak emission-line spectra, the weak-line or naked T Tauri stars, than for those with strong emission-line spectra, but the actual mass of those detected exhibits little correlation with strength of the emission lines. The disk masses range from less than $0.01\mathcal{M}_\odot$ to nearly $1\mathcal{M}_\odot$, with massive disks being very rare. There are few, if any, disks more massive than their central stars. The average mass of such disks is about $0.02(0.02/\kappa_\nu)\mathcal{M}_\odot$, sufficient to form planetary systems like the solar system.

The disks are cool, typically with temperatures of order 100 K at a distance of 1 AU from the stars. Many exhibit a flat spectrum, whose luminous output is almost independent of frequency over a wide range. These disks are characterized by temperatures proportional to the inverse square root of distance from the star. No disks appear to have radial temperatures varying more slowly than this dependence. The hottest ones are more luminous than the central stars. It is not obvious what the source of this luminosity can be; accretion or release of stored gravitational energy from the stars through magnetic fields are possible candidates.

Millimeter-wave spectral indices indicate disk particle emissivities which vary no faster than inversely with wavelengths near 1 mm. They are incompatible with emissivities varying inversely as the square of the wavelength, as is usually assumed for dust grains in the interstellar medium. Particle growth in the disks, perhaps as fractal dimension in linear size, is probably necessary to enhance the long-wavelength emissivities, and presents the possibility that one is witnessing particle growth perhaps in preplanetary nebulae.

The mass, size, and angular momentum of these disks are similar to those associated with the solar nebula during the first stage of planet formation. Because the disks are spatially thin, most of the matter is shielded from radiation pressure and mass loss from the stars, and it is likely that this matter can survive the known environments around T Tauri stars during their entire pre-main-sequence evolution. We find no evidence of dissipation over the timescales covered by our sample, up to 10^7 yr. Since no main-sequence stars are observed with disks of $0.01\mathcal{M}_\odot$ or more, the implication is that these are proto-planetary disks, and that planetary systems are common in the Galaxy. More extensive observations of a subset of the stars studied in this paper may reveal the nature of the process by which planets are born and give us insight into our own origins.

Many fruitful ideas and insights sprung from conversations with P. Cassan; it is a pleasure to thank him for these discussions. We also profited from discussions with S. Edwards, J. Houck, P. Hartigan, F. Shu, M. Skrutskie, K. Strom, and S. Strom and from comments by J. Emerson and an anonymous referee. The observations would have been impossible but for the generosity of P. Mezger in providing the bolometer, and we are grateful to the staff of IRAM for excellent support of the observations. This work was partially supported by the NSF through Grants No. AST 88-02458 to Cornell and Grant No. AST 87-14405 to Caltech, and by the Max-Planck Society.

REFERENCES

Abt, H. A., and Levy, S. G. (1976). Astrophys. J. Suppl. **30**, 273.
Adams, F. C., Emerson, J. P., and Fuller, G. A. (1990). Astrophys. J. (submitted).
Adams, F. C., Lada, C. J., and Shu, F. H. (1987). Astrophys. J. **312**, 788 (ALS).
Adams, F. C., Lada, C. J., and Shu, F. H. (1988). Astrophys. J. **326**, 865.
Avni, Y., Soltan, A., Tananbaum, H., and Zamorani, G. (1980). Astrophys. J. **238**, 800.
Baars, J. W. M., Hooghoudt, B. G., Mezger, P. G., and de Jonge, M. J. (1987). Astron. Astrophys. **175**, 319.
Backman, D. E., and Gillett, F. C. (1987). In *Cool Stars and Stellar Systems and the Sun*, edited by J. Linsky and R. E. Stencel (Springer Berlin), p. 340.
Backman, D. E., Gillett, F. C., and Witteborn, F. C. (1990). Astrophys. J. (submitted).
Bastien, P. (1982). Astron. Astrophys. Suppl. **48**, 153.
Beckwith, S., Sargent, A. I., Scoville, N. Z., Masson, C. R., Zuckerman, B., and Phillips, T. G. (1986). Astrophys. J. **309**, 755.
Beckwith, S. V. W., Sargent, A. I., Koresko, C. D., and Weintraub, D. A. (1989). Astrophys. J. **343**, 393.
Bertout, C., Basri, G., and Bouvier, J. (1988). Astrophys. J. **330**, 350.
Bieging, J. H., Cohen, M., and Schwartz, P. R. (1984). Astrophys. J. **282**, 699.
Chen, W. P., and Simon, M. (1988). Bull. Am. Astron. Soc. **20**, 955 (CS88).
Chen, W. P., and Simon, M. (1990). In preparation (CS90).
Chen, W. P., Simon, M., Longmore, A., Howell, R. R., and Benson, P. (1990). Astrophys. J. (submitted) (CSLHB90).
Cohen, M. (1983). Mon. Not. R. Astron. Soc. **173**, L69.
Cohen, M., Emerson, J. P., and Beichman, C. A. (1989). Astrophys. J. **339**, 455.
Cohen, M., and Kuhi, L. V. (1979). Astrophys. J. Suppl. **41**, 743 (CK79).
Draine, B. T. (1989). Proceedings of the 22nd and ESLAB Symposium Infrared Spectroscopy in Astronomy, edited by B. H. Kaldeich (ESA Publications, Noordwijk).
Draine, B. T., and Lee, H. M. (1984). Astrophys. J. **285**, 89.
Dyck, H. M., Simon, T., and Zuckerman, B. (1982). Astrophys. J. Lett. **255**, L103 (DSZ82).

Edwards, S., Cabrit, S., Strom, S. E., Heyer, I., Strom, K. M., and Anderson, E. (1987). Astrophys. J. **321**, 473.
Elias, J. H. (1978). Astrophys. J. **224**, 857.
Emerson, J. P. (1988), in *Formation and Evolution of Low Mass Stars*, edited by A. K. Dupree and M. T. V. Lago (Kluwer Academic), p. 21.
Evans, N. J., II, Levreault, R. E., Beckwith, S., and Skrutskie, M. F. (1987). Astrophys. J. **320**, 364.
Feigelson, E. D., and Kriss, G. A. (1981). Astrophys. J. Lett. **248**, L35.
Hartmann, L., Hewett, R., Stahler, S., and Mathieu, R. (1986). Astrophys. J. **309**, 275 (HHSM86).
Herbig, G. H., and Robbin-Bell, K. (1988). Lick Obs. Bull No. 1111 (HBC).
Hildebrand, R. H. (1983). R. Astron. Soc. **24**, 267.
Hodapp, K. -W. (1984). Astron. Astrophys. **141**, 255.
Jones, B. F., and Herbig, G. H. (1979). Astron. J. **84**, 1872 (JH79).
Joy, A. H., and Van Biesbroeck, G. (1944). Publ. Astron. Soc. Pac. **56**, 123 (JVB44).
Kenyon, S. J., and Hartmann, L. (1987). Astrophys. J. **323**, 714.
Kreysa, E. (1985). Proceedings of the URSI International Sympa. Millimeter and Submillimeter Wave Radio Astronomy, Granada, p. 153.
Lynden-Bell, D., and Pringle, J. E. (1974). Mon. Not. R. Astron. Soc. **168**, 603.
Marochnik, L. S., Mukhin, L. M., and Sagdeev, R. Z. (1988). Science **242**, 547.
Millman, P. M. (1975). In *Dusty Universe*, edited by G. B. Field and A. G. W. Cameron (Watson, New York), p. 185.
Mundt, R., Walter, F. M., Feigelson, E. D., Finkenzeller, U., Herbig, G. H., and Odell, A. P. (1983). Astrophys J. **269**, 229 (MWFFHO83).
Pringle, J. E. (1981). Annu. Rev. Astron. Astrophys. **19**, 137.
Rydgren, A. E., Schmelz, J. T., Zak, D. S., and Vrba, F. J. (1984). Publ. U. S. Nav. Obs. XXV, 1 (RSZV).
Sargent, A. I., and Beckwith, S. (1987). Astrophys. J. **323**, 294.
Sargent, A. I., and Beckwith, S. (1989). In *Structure and Dynamics of the Interstellar Medium*, IAU Colloquium No. 120, edited by Tenorio-Tagle, J. Melnick, and M. Moles (Springer, Berlin), p. 215.
Sargent, A. I., and Beckwith, S. (1990). In preparation.
Sato, S., Nagata, T., Nakajima, T., Nishida, M., Tanaka, M., and Yamashita, T. (1985). Astrophys. J. **291**, 708.
Smith, B. A., and Terrile, R. J. (1984). Science **226**, 1421.
Spitzer, L., Jr. (1978). *Physical Processes in the Interstellar Medium* (Wiley, New York), pp. 162, 163.
Strom, K. M., Strom, S. E., Edwards, S., Cabrit, S., and Skrutskie, M. F. (1989). Astron. J. **97**, 1451 (SSECS).
Strom, K. M., Strom, S. E., Wolff, S. C., Morgan, J., and Wenz, M. (1986). Astrophys. J. Suppl. **62**, 39.
Vandenberg, D. A. (1983). Astrophys. J. Suppl. **51**, 29.
Vogel, S. N., and Kuhi, L. V. (1981). Astrophys. J. **245**, 960.
Walter, F. M. (1987). Publ. Astron. Soc. Pub. **99**, 31.
Walter, F. M., Brown, A., and Vrba, F. J. (1990). Astrophys. J. (in press).
Walter, F. M., and Kuhi, L. V. (1981). Astrophys. J. **250**, 254.
Weintraub, D. A., Masson, C. R., and Zuckerman, B. (1989). Astrophys. J. **344**, 915.
Weintraub, D. A., Sandell, G., and Duncan, W. D. (1989). Astrophys. J. Lett. **340**, L69.
Wolstencroft, R. D., and Walker, H. J. (1988). Philos. Trans. R. Soc. London Ser. A, **325**, 423.
Woody, D. P., Scott, S. L., Scoville, N. Z., Mundy, L. G., Sargent, A. I., Padin, S., Tinney, C. G., and Wilson, C. D. (1989). Astrophys. J. Lett. **337**, L41.
Wright, E. L. (1987). Astrophys. J. **320**, 818.